OUKA
Osaka University Knowledge Archive

Title	電界放出型電子銃を用いた走査型電子顕微鏡における加速レンズ系の解析並びに設計
Author(s)	黒田, 勝廣
Citation	大阪大学, 1975, 博士論文
Version Type	VoR
URL	https://hdl.handle.net/11094/2489
rights	
Note	

Osaka University Knowledge Archive : OUKA

https://ir.library.osaka-u.ac.jp/

Osaka University

ANALYSIS AND DESIGN OF ACCELERATING LENS SYSTEM FOR FIELD EMISSION SCANNING ELECTRON MICROSCOPE

BY

KATSUHIRO KURODA

DEPARTMENT OF APPLIED PHYSICS,
FACULTY OF ENGINEERING,
OSAKA UNIVERSITY,
SUITA, OSAKA,
JAPAN

— DECEMBER 1974 —

報告番号 甲第1807号

論 文 目 録

黒 田 勝 広

主論文 Analysis and Design of Accelerating Lens System for Field Emission Scanning Electron Microscope
（電界放出型電子銃を用いた走査型電子顕微鏡における加速レンズ系の解析ならびに設計）

（主論文のうち印刷、公表したもの）

1. Aperture Effect of Electrostatic Lenses
（静電レンズのアパーチャ効果）
Japanese Journal of Applied Physics 11巻 8号
昭和47年 8月 5日

2. Potential and Field Analysis Method used Electrode Surface Charges
（電極表面電荷を用いたポテンシャルとフィールドの解析方法）
Japanese Journal of Applied Physics 11巻 9号
昭和47年 8月 5日

3. Electron Trajectory and Virtual Source of Field Emission Gun of SEM
（走査型電子顕微鏡の電界放出型電子銃の電子軌道とみかけの大きさ）
Japanese Journal of Applied Physics 11巻 9号

昭和47年 8月5日

4. Field Emission Scanning Electron Microscope with Parallel Plate Gun Electrodes

（平行平板電極をもった電界放出型電子銃を用いた走査型電子顕微鏡）

Proceedings of the Sixth Annual Scanning Electron Microscope Symposium, IITRI

昭和48年 4月

5. Analysis of Accelerating Lens System for the Field Emission Scanning Electron Microscope

（電界放出型電子銃を用いた走査型電子顕微鏡に対する加速レンズの解析）

Journal of Applied Physics 45巻3号

昭和49年 3月

6. Three Anode Accelerating Lens System for the Field Emission Scanning Electron Microscope

（電界放出型電子銃を用いた走査型電子顕微鏡に対する三陽極加速レンズ系）

Journal of Applied Physics 45巻 5号

昭和49年 5月

7. Three anode Accelerating Lens System for the Field Emission Scanning Electron Microscope (II)

（電界放出型電子銃を用いた走査型電子顕微鏡に対する三陽極加速レンズ系 (Ⅱ)）

Applied Physics Letters 25巻 1号

昭和49年 7月

8. Determination of the Spot Size by using the Intensity Distribution in the Accelerating Lens System of Scanning Electron Microscope

（走査型電子顕微鏡の加速レンズにおいて強度分布を用いたスポット径の決定）

Japanese Journal of Applied Physics 13巻10号

昭和49年 10月 5日

9. Effect of Eccentricity of Anodes in Accelerating Lens for Field Emission Scanning Electron Microscope

（電界放出型電子銃を用いた走査型電子顕微鏡に対する加速レンズにおける電極間の偏心の影響）

Japanese Journal of Applied Physics 13巻12号

昭和49年 12月 5日

（主論文のうち未公表のもの）

1. High Current Efficiency Accelerating Lens System for Field Emission Scanning Electron Microscope

（電界放出型電子鏡を用いた走査型電子顕微鏡に対する高電流効率加速レンズ）

Journal of Applied Physics 46巻1号

昭和50年 1月

JOURNAL OF APPLIED PHYSICS
APPLIED PHYSICS LETTERS
published by the American Institute of Physics

Editors
Lester Guttman (JAP)
Gilbert J. Perlow (APL)
Associate Editors
Thomas H. Braid (APL)
David C. Hess (JAP & APL)

SEP 27 1974

ARGONNE NATIONAL LABORATORY
Post Office Box 296
Argonne, Illinois 60439
Telephone (312) 739-7711
Ext. 2874

SCHEDULING NOTICE

To: Author

From: Editor

We are tentatively scheduling your paper, manuscript number C8077, to appear in the JAN 1975 issue of the JOURNAL OF APPLIED PHYSICS. Your manuscript has already been sent to our Publications Office in New York. Correspondence concerning your paper should hereafter include the full title and name(s) of the author(s) and should be addressed to:

Chief Copy Editor
Journal of Applied Physics
American Institute of Physics
335 East 45th Street
New York, New York 10017

Please do not send any changes in your manuscript to the Chief Copy Editor. You may make minor changes when you receive galley proofs. Major changes in galley proofs will be referred to the Editor for review.

afk

ANALYSIS AND DESIGN OF ACCELERATING LENS SYSTEM FOR FIELD EMISSION SCANNING ELECTRON MICROSCOPE

BY

KATSUHIRO KURODA

DEPARTMENT OF APPLIED PHYSICS,
FACULTY OF ENGINEERING,
OSAKA UNIVERSITY,
SUITA, OSAKA,
JAPAN

— DECEMBER 1974 —

A mes parents

ABSTRACT

The analysis and design of accelerating lens system which is indispensable for the operation of the Field Emission Scanning Electron Microscope (FESEM) are described.

The characteristics of the Butler type accelerating lens are compared with those of the flat-plate one which is the most simple lens. Although the spot sizes attainable with these lenses are almost the same, the current efficiency (or degradation) of the Butler type is better than that of the flat-plate lens by two times. This conclusion was confirmed experimentally.

A three anode accelerating lens is developed in the present investigation and also the characteristics and advantages are described in detail. This lens is actually a hybrid of the immersion and unipotential lenses. This lens has the advantage that the working distance of this lens can freely be changed under given conditions. This feature was confirmed by the computer simulation as well as the experiment. The experiment showed that the accelerating voltage could freely be changed without deteriolating the focussing. Moreover the computer simulation of the lens system composed of this three anode accelerating and the magnetic lenses has predicted that the current efficiency of this lens system is improved one order higher than that of conventional lens system (e.g. Butler type and magnetic lenses) in the region of beam current more than about 10^{-8} Amp.. In particular, it is shown that the spot size of less than 100 Å can be obtained for the beam current of 10^{-8} Amp..

The computer analysis has shown that the curved anode configuration can be replaced by the plane one of simplified version type without changing the characteristics. This has been confirmed in experiment with a three anode accelerating lens constructed for this purpose.

The electron trajectories emerging from the tip are also calculated by computer to estimate the virtual source size of the tip.

An intensity distribution of the electron beam on a specimen is computed by an electron wave optics approach, and the resultant spot size is discussed from this intensity distribution.

An influence of the eccentricity of electrostatic lenses on the spot size is analytically formulated and numerically calculated.

CONTENTS

CHAPTER 1 INTRODUCTION AND SUMMARY

The SEM invented by Knoll (1935) had been mainly developed by the workers of Cambridge Univ. in 1950s (Smith et al. 1955, Pease et al. 1965). In 1968 Crewe developed the SEM using a Field Emission gun (FESEM) and in 1970 his FESEM achieved the resolution of 5 Å.

A diagram outlining the SEM is shown in Fig. 1-1. The electron beam which is focused onto the specimen surface scans across the specimen surface in a rectangular raster in synchrony with the electron beam in the cathode ray tube (CRT). The signal (for example, secondary electron and backscattered electrons, see Fig. 1-2) generated at the specimen is amplified to be displayed on the CRT. Since much information of the specimen can easily be obtained by using the SEM, the SEM is one of the most useful tool in many fields of the science (for example, metallurgy, semi-conductor industry, chemistry, biology and medical science).

It is well known that the most important factor of SEM is the resolution. The resolution is closely related with the beam current, the lens aberrations and so on. The FE gun has , at present, been regarded as the most useful electron source because it has a high brightness and low energy spread, which guarantee a high resolution (see Table 1-1). When the FE gun is used, it is necessary for this gun to have at least two anodes. The potentials of the 1st and 2nd anodes give the field emission and accelerating voltages, respectively. The lens effect and aberrations are produced between these two anodes. This lens is called an accelerating lens. The Butler type accelerating lens (Butler 1966) was designed to have low aberrations, particularly, a small spherical aberration coefficient. Crewe has first developed the FESEM applying this Butler type accelerating lens. The schematic diagram of his SEM are shown in Fig. 1-3. After that, it was found that the chromatic aberration was dominant rather than the spherical aberration in the high resolution FESEM. Besides, the curved anode configuration used in Butler type lens is not easy to manufacture. Hence the various accelerating lenses have been investigated by many workers (for example, Fraser 1971, Munro 1972 and Tonomura 1973). However, the characteristics of the accelerating lens could not be improved remarkably. The reasons of this seem to be that the accelerating lenses are generally composed of two anodes and the characteristics of these lenses is strongly dependent on the ratio of the field emission and accelerating voltages.

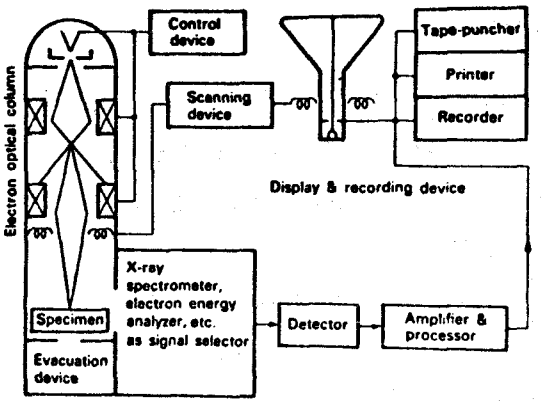

Fig. 1-1 Schematic diagram of the SEM.

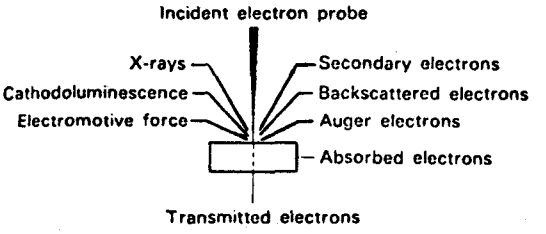

Fig. 1-2 Kinds of information carriers produced by the interactions between incident electrons and substances.

CATHODE TYPE	DATA SOURCE	PROBE DIAMETER (not resolution) d_{min}	PROBE CURRENT (ampere)	BRIGHTNESS A/cm²-ster (estimated value)	TYPICAL LIFE for GIVEN BRIGHTNESS	TEMP. (°k)	TYPICAL SATISFACTORY VACUUM LEVEL (mm Hg)
Tungsten hairpin (0.005")	Pease & Nixon J.Sci.Instr. 42(1965)31.	50Å 15mm focal length Surface or transmission microscopy	8×10^{-13}	7×10^{4}	30 hours	2859	5×10^{-4}
LaB_6 rod Shottky Emission (1 micron tip diameter)	Broers In SEM/1970 IITRI, Chicago, Ill., 1.	25Å (diffraction-aberration limited) 15mm focal length Surface or transmission	2×10^{-12}	6×10^{6}	100 hours (insufficient data)	2000	1×10^{-6}
Tungsten Field Emission tip	Crewe J.Mol.Biol. (1970)375.	5Å (diffraction-chromatic spherical aberration limited) 0.4mm focal length Transmission	10^{-10}	10^{9}	No limit however reconditioning required approximately every hour	Ambient	10^{-10}

Table 1-1 Comparison among the various electron sources.

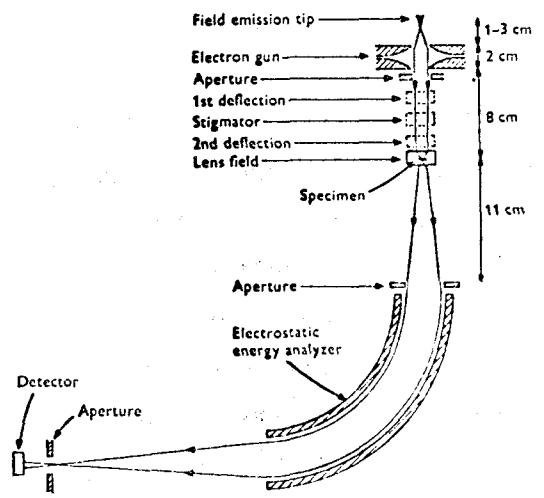

Fig. 1-3 Schematic diagram of the high resolution SEM. (Crewe 1970)

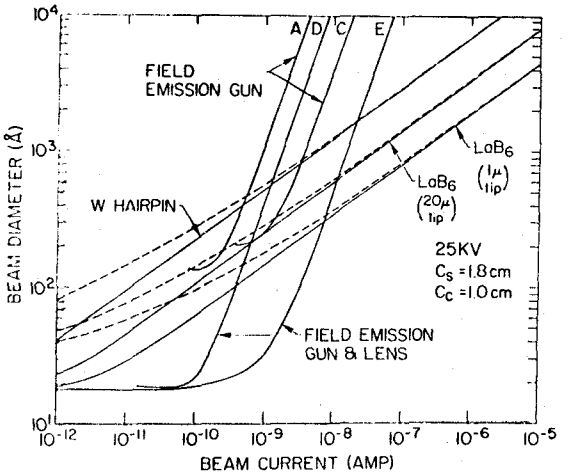

Fig. 1-4 Performances of thermal and field emission cathodes. (Broers 1972)

So Veneklasen and Siegel (1970 and 1972) proposed a method in which the first anode is replaced by an einzel lens, and Someya (1972 and 1974) proposed an accelerating lens composed of three anodes. These accelerating lenses have the advantage that the characteristics of these lenses are almost independent on the given physical restriction. However, these accelerating lenses are large in dimension and the aberrations also becomes larger in proportion to the dimension.

In SEM the high resolution is, of course, very important, however, Auger Electron Scanning Microscope (MacDonald 1970 and 1971) in which Auger electron intensity is displayed as SEM image on the CRT has actively been used, and the electron beam microfabrication has also been practiced with great interest (for example, Brewer 1971, Broers 1972 and Angello 1973). In these applications a higher current than about 10^{-8} Amp. and also high resolution ($10^{2} \sim 10^{3}$ Å) are needed. Although the FESEM can achieve very high resolution at the region of beam current less than 10^{-10} Amp., the probe size is tremendously increased for the region of beam current higher than about 10^{-9}Amp. (Broers 1973 and see Fig. 1-4). This reason is that the spherical and chromatic aberrations of the accelerating lens for larger aperture size become larger rapidly.

Considering the resolution, lens aberrations and secondary electron yield the FESEM is usually operated at accelerating voltages between 20 and 30 KV. However, recently the FESEM which can be operated in a range of lower or higher accelerating voltage has been required (Welter et al. 1972 and 1974, Veld et al. 1971, Shaffner 1971, and Someya et al. 1972 and 1974). For example, a micrograph of nonconducting specimens can be obtained without a conductive coating in a range of a low accelerating voltage (several hundred voltages). In the conventional FESEM it is impossible to change the accelerating voltage over a wide range, because the working distance of the accelerating lens changes according to the change of the accelerating voltage and this results in difficulty to obtain proper demagnification of the magnetic lens. Hence the probe size is directly affected by the aberrations of the accelerating lens, and consequently this incurs the enlargement of the probe size.

The high resolution under the condition of high beam current or of lower accelerating voltage which are an essential demand of the SEM, has still been required with great necessity. In this circumstance the investigation of the accelerating lens used in FE gun is most important.

So the present investigation is performed mainly to improve the defects of the conventional accelerating lens, and following improvements have been attained:

(1) The characteristics of the accelerating lens are scarcely dependent on the given physical restriction (for example, the field emission voltage, the accelerating voltage and the working distance).

(2) High current efficiency without losing high brightness of FE gun is obtained in the region of beam current more than about 10^{-8} Amp. Namely, the probe size is improved at least by one order in this current region.

(3) It is possible to manufacture the accelerating lens more easily.

These improvements were achieved by using the three anode accelerating lens with the plane anode configurations of simplified version type suggested in the present investigation, and the computer simulations and the experimental results have shown that this lens would be most hopeful at present. The contents of the present thesis are summarized chapter by chapter as follows.

In Chap.2 the theories and their numerical calculation methods of the geometrical electron optics which are necessary to analyze and design the accelerating lens are described, and also the methods of the evaluations of the electron probe size (spot size) and of its beam current on the specimen are described. The spot size is expressed by the combination of four factors (spherical and chromatic aberrations, diffraction effect and virtual source size). In particular the analysis and calculation methods for studying the potential and field of the electrostatic lens by using electrode surface charges are presented in Sec. 2-2-2.

In Chap. 3 the characteristics of the Butler type accelerating lens are compared with those of the flat-plate one, which is the most simple lens. It is discussed that the anode aperture effect can be neglected in the Butler type accelerating lens , however, this cannot be neglected in the flat-plate one. Although the spot size attainable with these lenses are almost the same, the current efficiency (or degradation) of the Butler type is better than that of the flat-plate lens by two times. This conclusion was confirmed experimentally by the prototype FESEM built by joint research between Osaka University and JEOL Ltd. The computer analysis has also shown that the curved anode configuration can be replaced by the plane one of simplified version type without changing the characteristics.

In Chap. 4 a three anode accelerating lens which is suited in the present purposes is developed in the present investigation, and its characteristics and advantages are described in detail. This lens is actually a hybrid of the immersion and unipotential lenses. This lens has the advantage that the working distance of the lens can freely be changed under given conditions (for example, the field emission voltage, the accelerating voltage and the working distance). This feature was confirmed by the computer simulation as well as the experiment. The experiment showed that the accelerating voltage could freely be changed without deteriolating the focussing. Moreover the computer simulation has predicted that the whole lens system composed of this lens and the magnetic lens could be operated under the optimum condition. Consequently the current efficiency of this lens system is improved one order higher than that of conventional lens system (e.g. Butler type and magnetic lenses) in the region of beam current more than about 10^{-8} Amp. In particular, it is shown that the spot size of less than 100 Å can be obtained for the beam current of 10^{-8} Amp.. Some problems in the manufacturing and operating conditions are also discussed.

In Chap. 5 some problems in the estimation of the spot size are discussed.

The virtual source size of the FE gun is formulated in Chap. 2. However, this estimation is based on an oversimplified and unrealistics model. So a sphere-on-orthogonal-cone model which is suggested by Dyke (1953) and has already been analyzed in detail by Wiesner and Everhart (1970 and 1973) is used to overcome this limitation and the virtual source size is estimated.

The estimation formula of the spot size which has been used conventionally is not based on the physical substantiality, so the spot size is estimated by the introduction of the electron wave optics approach.

The effects of an eccentricity of anodes which are very important in actual manufacturing and setting are theoretically formulated and numerically estimated.

In Chap. 6 the results obtained by the present investigation are summarized.

CHAPTER 2 GEOMETRICAL ELECTRON OPTICS

§ 2-1 Introduction

Theories of the geometrical electron optics have been studied for a long time, and nowadays the numerical calculations of them have mainly been performed by the electronic computer. In this chapter the theories and numerical calculation methods for the analysis of the accelerating lens system are described. In the first place, theories and the numerical calculation methods necessary to analize the potential and field in the space among the electrodes of the given configurations are described. In particular the analysis and calculation methods for the potential and field used electrode surface charges were developed in this investigation and are shown in Sec.2-2-2. The accuracy in this method is still not satisfactory, but this method have some advantages. In Sec.2-3 an analysis of electron trajectories and lens aberrations are described, and the estimation methods of the spot size and the current for the electron beams on to the specimen are shown in Sec.2-4. These analysis are very important to see the characteristics of the accelerating lens system. The more detailed theories and calculation procedures are shown in many books (EL-Kareh et al 1970, Grivet 1965, Pierce 1949, Septier 1967 and Zworykin 1945).

§ 2-2 Analyses of the potential and field

In electron optics it is important to know the position of the electrons in the space among electrodes of given configurations and potentials as a function of time. The problem can be divided into two parts; determination of the potential and field between the electrodes and the solutions in this field. In this section the former is described. The latter will be described in Sec.2-3. The solutions of the potential and field can be found by various methods as follows.

1) Purely mathematical calculation of the potential, field and the trajectories.
2) The rubber membrane.
3) Conductive paper.
4) The electrolytic tank.
5) Numerical methods. etc.

However the method of 1) is seldom applied except for the particular boundary conditions.

At present the numerical methods are most popular among these methods, because the electronic computer is developped tremendously and the solutions of the problems are calculated more accurately than any other methods. The established method of the numerical methods for the potential analysis seems to be only the mesh method. In this investigation the author developed also a method used electrode surface charges as shown in Sec.2-2-2. In the following, these method is described in detail.

§ 2-2-1 Mesh method

I) Theory and calculation procedure for the computer simulation (Weber 1962/1963 and Septier 1967)

The potential and field can be calculated from Poisson's equation as well known. Poisson's equation with rotational symmetry is given by,

$$\frac{\partial^2 V}{\partial r^2}+\frac{1}{r}\frac{\partial V}{\partial r}+\frac{\partial^2 V}{\partial z^2}=-\frac{\varrho}{\varepsilon_0} \quad , \qquad (2\text{-}1)$$

where the z axis is the axis of rotational symmetry, r is the distance to this axis, V is the potential, ρ is the space charge, which is a given function of r and z, and ε_0 is the dielectric constant of free space (see Fig.2-1). For solving this kind of problem numerically, use can best be made of difference equations. For this purpose we express the derivatives of V at a point P_0 in terms of the potential V_0 of P_0 and in terms of the potentials of nearly points whose distances h to P_0 are so small that we can permissibly neglect the terms to the third and higher powers of h in the series presently to be given. We distinguish between two cases ; P_0 not on the Z axis, and P_0 on the Z axis.

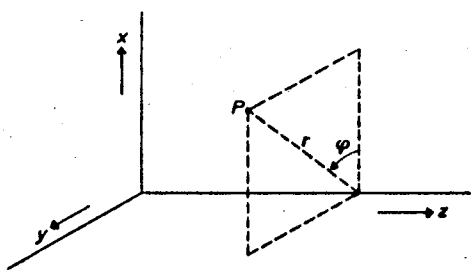

Fig. 2-1 Point P with rectangular coordinates x, y and z, and with cylindrical coordinates r, φ and z.

Difference equations

Point P_0 not on the Z axis. (see Fig. 2-2)

$$\frac{2}{h_1(h_1+h_2)}V_1+\frac{2}{h_2(h_1+h_2)}V_2+\frac{2r_0+h_4}{h_3(h_3+h_4)r_0}V_3+$$
$$+\frac{2r_0-h_3}{h_4(h_3+h_4)r_0}V_4=-\frac{\varrho_0}{\varepsilon_0}+\left[\frac{2}{h_1h_2}+\frac{2r_0+h_4-h_3}{h_3h_4r_0}\right]V_0 \qquad (2\text{-}2)$$

Particulary, in the case of $h_1=h_2=h_3=h_4=h$,

$$V_1+V_2+\left(1+\frac{h}{2r_0}\right)V_3+\left(1-\frac{h}{2r_0}\right)V_4=-\frac{\varrho_0 h^2}{\varepsilon_0}+4V_0 \quad . \tag{2-3}$$

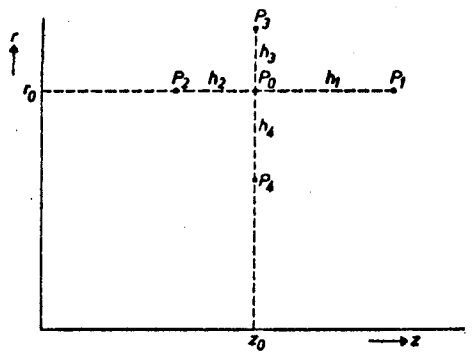

Fig. 2-2 Point P_0 at a distance r_0 from the z axis surrounded by points P_1, P_2, P_3 and P_4 at distances h_1... h_4 from P_0.

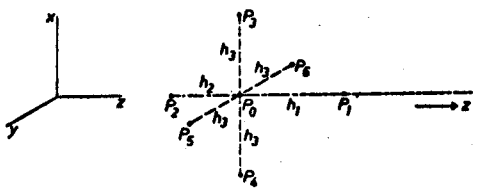

Fig. 2-3 Point P_0 on the z axis, surrounded by the six points P_1....P_6 at distances h_1, h_2 and h_3 from P_0.

Point P_0 on the Z axis (see Fig.2-3),

$$\frac{2}{h_1(h_1+h_2)}V_1+\frac{2}{h_2(h_1+h_2)}V_2+\frac{4}{h_3^2}V_3=-\frac{\varrho_0}{\varepsilon_0}+\left(\frac{4}{h_3^2}+\frac{2}{h_1h_2}\right)V_0 \quad . \tag{2-4}$$

Particulary in the case of $h_1=h_2=h_3=h$,

$$V_1+V_2+4V_3=-\frac{\varrho_0 h^2}{\varepsilon_0}+6V_0 \quad . \tag{2-5}$$

From these equations, the potential can be calculated by using the iterative technique (see Fig.2-4).

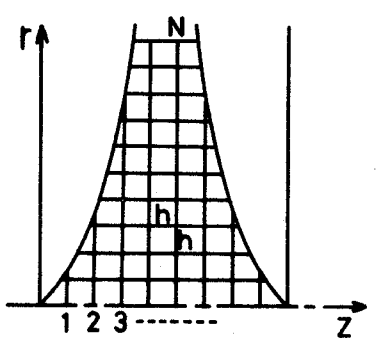

Fig. 2-4 The model used in mesh method. (Butler type accelerating lens)

The detailed calculation procedure and technique are omitted because they are described in many books in detail (for example, Weber 1962/63, and Septier 1967). In this technique we generally use a successive over-relaxation method (SOR method) to make the process converge faster, thus the number of cycles can be reduced. We denote the potential found for this

point after k cycles by $V_i^{(k)}$, and that found for k+1 cycles by $V_i^{(k+1)}$. This method is that the value of

$$V_i^{(k)} + w[V_i^{(k+1)} - V_i^{(k)}] \tag{2-6}$$

is substituted instead of $V_i^{(k+1)}$. The value of w must be carefully chosen. This optimum value depends only on the configuration of the electrodes, and not on the potentials initially adopted. The best value of w is also independent of the cycle number k. In this report Carre's method (Carre 1961) is used as described in the following.

1) The very first iteration is performed using a value of w of unity.

2) The next twelve iterations are performed using a value of w of 1.375. Then w can be obtained as follows using the Aitken-extrapolation.

$$p^{(k)} = \frac{\vec{n}^{(k)}}{\vec{n}^{(k+1)}} \quad , \tag{2-7}$$

where

$$\vec{n}^{(k)} = ||V_i^{(k+1)} - V_i^{(k)}|| \quad , \tag{2-8}$$

$$\lambda_{max} = p^{(k-2)} - [p^{(k-1)} - p^{(k-2)}]^2 / [p^{(k-2)} + p^{(k)} - 2p^{(k-1)}] \quad , \tag{2-9}$$

$$w_o = 2\{1 + [1 - (\lambda_{max} + w - 1)^2 / \lambda_{max} w^2]^{1/2}\} - 1 \quad . \tag{2-10}$$

3) The next iteration is performed using a value of w of Eq. (2-11).

$$w = w_o - (2 - w_o)/4 \tag{2-11}$$

4) Then, w_o is deemed satisfactory if the arithmetic difference Δw_o between this estimate and the previous one satisfies the condition;

$$\Delta w_o / (2 - w_o) < 0.05 \quad . \tag{2-12}$$

If Eq. (2-12) is not satisfied, 2) and 3) are iterated until Eq.(2-12) is satisfied. Thus, a final estimated value of w_o is obtained.

By the above mentioned procedure the potential can be calculated numerically. However this potential is only on the mesh points. So the potential on the arbitrary point is calculated by using the 5-point interpolation method. In this report the potentials are not used except for on the axial point, so this method is described only in the one-dimension. If the value on the mesh point z_0 is set f_0, the values on the arbitrary point are as follows.

$$f(z) = f_0 + [df/dz]_0(z-z_0) + 1/2[d^2f/dz^2]_0(z-z_0)^2 + 1/6[d^3f/dz^3]_0(z-z_0)^3 + 1/24[d^4f/dz^4]_0(z-z_0)^4 \quad , \quad (2\text{-}13)$$

$$f'(z) = [df/dz]_0 + [d^2f/dz^2]_0(z-z_0) + 1/2(d^3f/dz^3]_0(z-z_0)^2 + 1/6[d^4f/dz^4](z-z_0)^3 \quad , \quad (2\text{-}14)$$

$$f''(z) = [d^2f/dz^2]_0 + [d^3f/dz^3]_0(z-z_0) + 1/2[d^4f/dz^4](z-z_0) \quad , \quad (2\text{-}15)$$

where $[df/dz]_0$. $[d^2f/dz^2]_0$, are shown in Table 2-1.

case Ⅰ	−2 −1 0 1 2	$[df/dz]_0$	$(f_{-2}-8f_{-1}+8f_1-f_2)/12$
		$[d^2f/dz^2]_0$	$(-f_{-2}+16f_{-1}-30f_0+16f_1-f_2)/12$
		$[d^3f/dz^3]_0$	$(-f_{-2}+2f_{-1}-2f_1+f_2)/2$
		$[d^4f/dz^4]_0$	$(f_{-2}-4f_{-1}+6f_0-4f_1+f_2)/24$
case Ⅱ	−0 0 1 2 3	$[df/dz]_0$	$(-3f_{-1}-10f_0+18f_1-6f_2+f_3)/12$
		$[d^2f/dz^2]_0$	$(11f_{-1}-20f_0+6f_1+4f_2-f_3)/12$
		$[d^3f/dz^3]_0$	$(-3f_{-1}+10f_0-12f_1+6f_2-f_3)/2$
		$[d^4f/dz^4]_0$	$(f_{-1}-4f_0+6f_1-4f_2+f_3)$
case Ⅲ	−3 −2 −1 0 1	$[df/dz]_0$	$(-f_{-3}+6f_{-2}-18f_{-1}+10f_0+3f_1)/12$
		$[d^2f/dz^2]_0$	$(-f_{-3}+4f_{-2}+6f_{-1}-20f_0+11f_1)/12$
		$[d^3f/dz^3]_0$	$(f_{-3}-6f_{-2}+12f_{-1}-10f_0+3f_1)/2$
		$[d^4f/dz^4]_0$	$(f_{-3}-4f_{-2}+6f_{-1}-4f_0+f_1)$
case Ⅳ	0 1 2 3 4	$[df/dz]_0$	$(-25f_0+48f_1-36f_2+16f_3-3f_4)/12$
		$[d^2f/dz^2]_0$	$(35f_0-104f_1+114f_2-56f_3+11f_4)/12$
		$[d^3f/dz^3]_0$	$(-5f_0+18f_1-24f_2+14f_3-3f_4)$
		$[d^4f/dz^4]_0$	$(f_0-4f_1+6f_2-4f_3+f_4)$
case Ⅴ	−4 −3 −2 −1 0	$[df/dz]_0$	$(-3f_{-4}-16f_{-3}+36f_{-2}-48f_{-1}+25f_0)/12$
		$[d^2f/dz^2]_0$	$(11f_{-4}-56f_{-3}+114f_{-2}-104f_{-1}+35f_0)/12$
		$[d^3f/dz^3]_0$	$(3f_{-4}-14f_{-3}+24f_{-2}-18f_{-1}+5f_0)/2$
		$[d^4f/dz^4]_0$	$(f_{-4}-4f_{-3}+6f_{-2}-4f_{-1}+f_0)$

Table 2-1 Differential coefficients in 5-points interpolation method.

II) Accuracy and discussion

The accuracy of mesh method was examined against the Butler type accelerating lens as shown in Fig. 2-5. The NEAC 2200-model 500 computer was used to examine this accuracy. As for the potential, the accuracy better than 2.0×10^{-5} could be obtained within the calculation time of three minutes. It is generally considered that the defects of this method are with respect to the calculation time and the round off error produced by the iterative calculation. The another important problem is that the open boundary must be artificially transformed into the closed boundary and its boundary values are also given artificially. In this model used to examine the accuracy, however, the effect of the latter was sufficiently small. So the high accuracy could be obtained. As for the field, which was calculated by 5-point interpolation method, the accuracy better than 6.3×10^{-4} could be obtained.

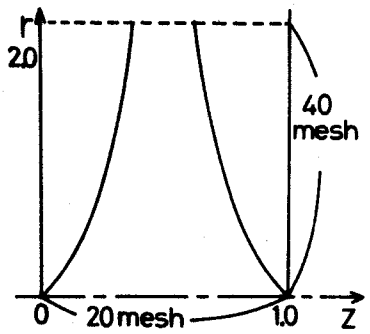

Fig. 2-5 The model used for examining the accuracy of the mesh method.

§ 2-2-2 Potential and field analysis method by using electrode surface charges

With respect to the potential and the field analysis, the established method seems to be only the mesh method as described in the previous section. Recently, however, B. Singer and M. Brawn (1970) suggested the analysis method used Green's function. In this section the analysis method using electrode surface charges is shown.

I) Theory and calculation procedure

The potential at the observation point (r_0, z_0) is expressed by the following equation in the cylindrical co-ordinates.

$$\phi(r_0, z_0) = 1/\pi\varepsilon \int \rho(r,z) K(t) r / [(z-z_0)^2 + (r+r_0)^2]^{1/2} dr\, dz \quad , \quad (2\text{-}16)$$

where

ε: dielectric constant,

$$t^2 = 4rr_0/[(z-z_0)^2 + (r+r_0)^2] \quad , \tag{2-17}$$

k(t): the complete elliptic integral of the first kind,

$\rho(r, z)$: charge density.

In the electrostatic electron lenses which has no space charge, charges are restricted on the electrode surfaces. Then, if a function which express the electrode surface configuration, is set

$$r = f(z) \quad , \tag{2-18}$$

$$f(r, z) = \rho(z) \cdot \delta(r - f(z)) \quad . \tag{2-19}$$

Then, Eq. (2-16) is reformed into

$$\phi(r_0, z_0) = 1/\pi\varepsilon\int\rho(z)rK(t)/[(z-z_0)^2 + (r+r_0)^2]^{1/2}dz \quad . \tag{2-20}$$

For the numerical computation, $\rho(z)$ is expanded in Chebysheff polynominal series,

$$\rho(z(x)) = \Sigma_{i=0}^{n} a_i T_i(x) \quad , \tag{2-21}$$

and also

$$(1-x^2)^{1/2}rK(t)/[(z-z_0)^2 + (r+r_0)^2]^{1/2}\, dz/dx = \Sigma_{j=0}^{n} b_j T_j(x) \quad . \tag{2-22}$$

Then, Eq. (2-20) is reformed into

$$\phi(r_0,z_0) = \pi a_0 b_0 + \pi/2\Sigma_{i=1}^{n} a_i b_i \quad , \tag{2-23}$$

by using orthogonality of Chebysheff polynominal. This Eq. (2-23) is used for the numerical computation. First a_i's values equivalent to $\rho(z)$ are unknown. So the observation point (r_0, z_0) is restricted on the

boundaries of the electrode surfaces, and (r_0, z_0) is scanned on them. Then the simultaneous linear equations are obtained and their solutions result in a_i's. Next (r_0, z_0) is fixed at an arbitary point which we want to know, then $\phi(r_0, z_0)$ can be calculated by using the known a_i's. The reason, why Chebysheff polynominal series for the numerical calculation is used, is that the accuracy and the calculation time of the numerical calculation are well improved by using the orthogonality and the special zero points of Chebysheff polynominal. [The detailed calculation procedure and technique are omitted on account of limited space. See the paper of Torii and Makinouchi(1968).]

Now, there is a gross problem that the potentials on the points of the existing charges diverge infinitely. This corresponds to t=1 and $k(t) \to \infty$ in the case of $(r, z) = (r_0, z_0)$ in Eq. (2-16). However,

$$\lim_{t\to 1} K(t) = 1/2 \log 16/(1-t^2) \quad , \tag{2-24}$$

and

$$\lim_{t\to 1} (1-t) \log (1-t^2) = \lim_{t\to 1} (1-t)^{1/2} 4t/(1+t) \to 0 \quad . \tag{2-25}$$

Eq. (2-25) shows that this problem may be neglected from the nature of the improper integral and consequently there is no problem in the use of Chebysheff polynominal series and this technique is superior to the curvilinear integral used by B. Singer et al. with respect to the problem of the singularity and the numerical calculation.

In this method the field of the observation point can be also calculated directly. The formulae of the field calculation are shown as following.

$$\frac{\partial \phi}{\partial r_0} = \frac{1}{\pi\varepsilon}\{- \int \frac{\rho(z)\ r\ (r+r_0)\ E(t)\ dz}{[(z-z_0)^2 + (r+r_0)^2]^{3/2}(1+t^2)}$$

$$+ 2 \int \frac{\rho(z)\ r\{E(t)-(1-t^2)K(t)\}dz}{[(z-z_0)^2 + (r+r_0)^2]^{3/2} t^2 (1-t^2)} \} \quad , \tag{2-26}$$

$$\frac{\partial \phi}{\partial z_0} = \frac{1}{\pi \varepsilon} \int \frac{\rho(z)\ r\ (z-z_0)\ E(t)\ dz}{[(z-z_0)^2 + (r+r_0)^2]1/2[(z-z_0)^2 + (r-r_0)^2]} \quad , \tag{2-27}$$

where E(t): the complete elliptic integral of the second kind.

II) Accuracy and discussion

The accuracy of this method is checked by using the Butler type accelerating lens (see Fig. 2-5). In this case a problem is occurred that how many numbers of the terms of Chebyseff polynominal series and the sample points of (r_0, z_0) in Eq. (2-22) should be selected. It was found that when the latter is twice as many as the former, the potential and the field could be calculated more accurately than under any other conditions. The results are shown in Table 2-2 together with those obtained by the mesh method. In this table when the number of the terms is more than 40, the simultaneous liner equation becomes ill condition and the potential and field could not be calculated, because the physical values between the sample points become to have the relation of the linearly dependent. From this table both the accuracy and the calculation time of this method are inferior to them of the mesh method. However, this method has merits such as follows.

1) This method can be dealt with open boundaries.
2) The potential and field at an arbitary point can directly be obtained.

Number of the term	16	20	26	30	36	40	mesh method
Number of the sample points	31	51	51	61	76	76	
Calculation time (minuts)	0.7	1.2	1.8	2.7	3.9	4.8	3.0
Accuracy (potential)	1.5×10^{-3}	7.2×10^{-3}	8.2×10^{-4}	6.0×10^{-4}	3.6×10^{-4}	——	2.0×10^{-5}
Accuracy (field)	5.7×10^{-3}	1.0×10^{-2}	8.0×10^{-3}	6.6×10^{-3}	4.6×10^{-3}	——	6.3×10^{-4}

Table 2-2 The comparison of the method used electrode surface charges with the mesh method.

§ 2-3 Analyses of electron trajectory and lens aberrations

The potential and field in the lens region has been solved in the r-z plane by using the method shown in the previous section. In this section the equations of motions of electrons and lens aberration coefficients are dealt with. In electron optics it is very important to know the positions of the electrons and also the effects of its aberrations. These aberrations can arise for a number of different reasons.

If the accelerating potential and the lens excitations fluctuate about their mean values, "chromatic aberration" will mar the image. If the properties of the system are investigated, using a more exact approximation to the refractive index than in employed in the Gaussian approximation, we can find that "geometrical aberrations" affect both the quality and the fidelity of the Gaussian image. When the properties of the system are analyzed using the nonrelativistic approximation, the disparities between the relativistic and nonrelativistic results can, for accelerating potential up to about 100KV, be conveniently regarded as a "relativistic aberration". If, finally, the properties of the system are calculated on the assumption that mechanically, the system is perfect - that the machining and alignment of all its parts are faultless - the properties of any real system will disagree, to a greater or lesser extent with calculated values; this we call the "mechanical aberration". These are the most important types of aberrations in electron optical system. moreover there are regions where the electron current density is very high; in such system, the "space-charge aberration" produced by the interaction between the electron charges may have to be considered.

In this section we will be concerned primarily with the geometrical aberrations (particularly spherical aberration) and the chromatic aberration. Because in the geometrical aberrations the aberrations except for the spherical aberration are all zero as concerns the electrons emerging from the axial points, and in this investigation the electrons may be considered as emerging from the axial points. As those theories and the calculation methods are described in many books (for example, Grivet 1965, Septier 1967) in detail, they are shortly discussed in this thesis.

When the space charge is neglected, the potential $\phi(r, z)$ satisfies the Laplace's equation and is expressed in cylindrical coordinates as follows:

$$\frac{\partial^2\phi}{\partial r^2}+\frac{1}{r}\frac{\partial\phi}{\partial r}+\frac{\partial^2\phi}{\partial z^2}=0. \qquad (2\text{-}28)$$

The solution of Eq. (2-28) can be expressed with the axial potential $\Phi(z)$ by

$$\phi(r,z)=\sum_{n=0}\frac{(-1)^n}{(n!)^2}\Phi^{2n}(z)\left(\frac{r}{2}\right)^{2n}. \tag{2-29}$$

This formula impies that the anode configulations may be calculated from the axial potential. If the third-order spherical aberration coefficient C_s and the first-order chromatic aberration coefficient C_c are dominant, the respective aberration coefficients can be calculated using the axial potential by

$$C_s=\frac{1}{16(\Phi_0)^{1/2}}\int_{z_0}^{z_1}\Phi^{1/2}r^4\left[\frac{5}{4}\left(\frac{\Phi''}{\Phi}+\frac{\Phi'}{\Phi}\frac{r'}{r}-\frac{\Phi'^2}{\Phi^2}\right)^2 + \frac{\Phi'^2}{\Phi^2}\left(\frac{r'}{r}+\frac{7}{8}\frac{\Phi'}{\Phi}\right)^2+\frac{1}{64}\frac{\Phi'^4}{\Phi^4}\right]dz, \tag{2-30a}$$

or

$$C_s=\frac{1}{16(\Phi_0)^{1/2}}\int_{z_0}^{z_1}\Phi^{-3/2}r^4\left(\frac{5}{4}\Phi''^2+\frac{5}{24}\frac{\Phi'^4}{\Phi^2}+\frac{14}{3}\frac{\Phi'^3}{\Phi}\frac{r'}{r}-\frac{3}{2}\Phi'^2\frac{r'^2}{r^2}\right)dz, \tag{2-30b}$$

$$C_c=\frac{\Phi_a}{(\Phi_0)^{1/2}}\int_{z_0}^{z_1}\frac{3}{8}\frac{\Phi'^2}{\Phi^{5/2}}r^2dz, \tag{2-31}$$

where Φ_0 and Φ_a are the potentials on the object side and the image side, respectively. The electron trajectory r=r(z) in the above equations satisfies the paraxial ray equation

$$\frac{d^2r}{dz^2}+\frac{\Phi'}{2\Phi}\frac{dr}{dz}+\frac{\Phi''}{4\Phi}r=0, \tag{2-32}$$

with an initial condition that the trajectory intersects the axial at $z=z_0$ (where the object plane intersects the z axis) with a slope of unity, $(dr/dz)_{z=z_0}=1$, as shown in Fig. 2-6. These aberration coefficients are referred back to the object side.

The numerical calculation method are Runge-Kutta method for Eq. (2-32) and Simpson's 1/3 rule for Eqs. (2-30a), (2-30b) and (2-31). These methods are well known (see Septier 1967), so they are omitted in this thesis.

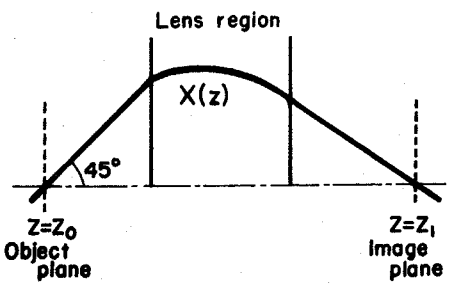

Fig. 2-6 Characteristics ray of Gaussian optics.

§ 2-4 Evaluation functions of the lens system

In the lens system it is most important to know the evaluation functions for the analysis and designs of the lens characteristics. There are two main parameters in the evaluation of the lens system of the SEM. The one is the spot size which is the spread of the electron beam on the specimen, and the other is the beam current. The spot size is mainly determined by the spherical aberration, chromatic aberration, the diffraction effect at the limting aperture and the virtual source size.

In the following, these are formulated. The model and the notations used are shown in Fig. 2-7, and Table 2-3.

I) Accelerating lens

The spherical and chromatic aberration coefficients are referred back to the source side as shown in Sec. 2-3. The spread due to the spherical aberration is expressed by the diameter

$$d_{Cs}=2/4MC_s\alpha_0^3=0.5M^4C_s\alpha_1^3(V_0/V_1)^{3/2}, \quad (2\text{-}33)$$

of the circle of least confusion on the specimen, and the spread due to the chromatic aberration is given by

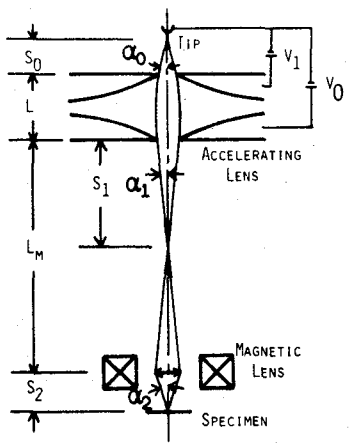

Fig. 2-7 Schematic diagram of FESEM.

$$d_{Cc}=2C_c\alpha_0M\Delta V/V_0=2C_c\alpha_1M^2\Delta V/V_0(V_0/V_1)^{1/2} \quad , \quad (2\text{-}34)$$

where

$$M=(V_1/V_0)^{1/2}\alpha_0/\alpha_1 \quad , \quad (2\text{-}35)$$

is the magnification.

The spreads d_d due to the diffraction at the limiting aperture and d_s due to the virtual source size also contribute to the spread of the electron beam on the specimen and are expressed by

$$d_d=1.22\lambda/\alpha_1 \quad , \quad (2\text{-}36)$$

$$d_s=Mr_s=2MR(V_T/V_1)^{1/2} \quad , \quad (2\text{-}37)$$

where

$$r_s=2R(V_T/V_1)^{1/2} \quad , \quad (2\text{-}38)$$

Accelerating lens

M ; magnification
V_1 ; field emission voltage
V_0 ; accelerating voltage
α_0 ; incident half-angle of the electron beam
α_1 ; exit half-angle of the electron beam
C_s ; spherical aberration coefficient (referred back to the source)
C_c ; chromatic aberration coefficient (referred back to the source)
ΔV ; total energy spread
V_T ; transverse energy spread of the electron leaving the tip
λ ; wavelength of the electron beam
d_s ; virtual source size
d_d ; diffraction effect
d_{Cs} ; spherical aberration
d_{Cc} ; chromatic aberration
S_0 ; distance between the tip and the first anode
S_1 ; working distance
L ; distance between the anodes
R ; radius of the tip curvature
d ; spot size
α_1^0 ; optimum half angle of α_1 for which d is minimum
a_p ; aperture size located under the lens system
I_s ; the emission current emerging from the tip per steradian
I_0 ; total current emerging from the tip
I ; current on the specimen
B ; brightness

Auxiliary magnetic lens

M_m ; magnetic lens
S_2 ; working distance
L_m ; distance between the last anode of the accelerating lens and the magnetic lens
α_2 ; exit half-angle of the electron beam
C_{sm} ; spherical aberration coefficient (referred back to the specimen)
C_{cm} ; chromatic aberration coefficient (referred back to the specimen)
d_{Csm} ; spherical aberration
d_{Ccm} ; chromatic aberration
d_{dm} ; diffraction effect
d_m ; spot size

Table 2-3 List of the notations

is the virtual source size which was analytically formulated by Ruska and Everhart (Ruska 1933 and Everhart 1967) for the spherical model as the electron source. However, it doesn't seem that this model is based on the actual tip as an electron source in SEM. So in Sec 5-1 the better approximation than this model will be shown. Combining the above four factors, we can express the spot size d of the electron beam on the specimen by

$$d=(d_s^2 + d_{Cs}^2 + d_{Cc}^2 + d_d^2)^{1/2} \quad . \qquad (2\text{-}39)$$

Here α_1 must be determined to estimate d and the smaller α_1 is the smaller d_{Cs} and d_{Cc} will be. However, d_d becomes larger the smaller α_1 is. Then it is possible to determine the optimum α_1^0 for which d is minimum, and the optimum α_1^0 is expressed by

$$\alpha_1^o=\frac{[-4C_c^2(\Delta V/V_2)^2+\{16(\Delta V/V_2)^4C_c^4+4.4652\lambda^2C_s^2(V_2/V_1)\}^{1/2}]^{1/4}}{(3/2)^{1/4}M^2C_s^{1/2}(V_2/V_1)^{3/4}} \quad . \qquad (2\text{-}40)$$

In the expression Eq. (2-39) of the spot size, there is no physical substantiation. So in the Sec. 5-2, this point will be discussed. The beam current I on the specimen can be estimated approximately by

$$I = \pi\alpha_0^2 I_s = \pi M^2 (V_0/V_1)\alpha_1^2 I_s \quad , \qquad (2\text{-}41)$$

$$I_s = I_0/4\pi \quad , \qquad (2\text{-}42)$$

The brightness B is expressed from the definition by

$$B = I/\pi^2 d^2 \alpha_1^2 \quad , \qquad (2\text{-}43)$$

on the specimen.

II) Auxiliary magnetic lens

The spherical and chromatic aberration coefficients are refered back to the specimen side, so the spherical and chromatic aberrations are expressed by

$$d_{Csm} = 0.5\, C_{sm}\alpha_2^3 \quad , \qquad (2\text{-}44)$$

$$d_{Ccm} = 2C_{cm}\alpha_2\Delta V/V_2 \quad . \qquad (2\text{-}45)$$

The diffraction effect at the limiting aperture is also expressed by

$$d_{dm} = 1.22\lambda/\alpha_2 \quad . \qquad (2\text{-}46)$$

When an auxiliary magnetic lens is used in order to magnify or demagnify the image produced by the electron gun and the accelerating lens, and the limiting aperture is set at the magnetic lens region, we can express the spot size d_m of the electron beam on the specimen by

$$d_m = \{M_m^2 (d_{Cs}^2 + d_{Cc}^2 + d_s^2) + d_{Csm}^2 + d_{Ccm}^2 + d_{dm}^2 \}^{1/2} \quad , \qquad (2\text{-}47)$$

where

$$M_m = \alpha_1/\alpha_2 = S_2/(L_m - S_1) \qquad (2\text{-}48)$$

is the magnification of the magnetic lens.

§ 2-5 Discussion

In this chapter the elementary theories and numerical calculation procedures for the evaluation of accelerating lens were individually described. These are performed with the process as shown in Fig. 2-8 and as follows.

(1) The parameters of the lens and needful physical constants of others are set.

(2) The potential and field in the lens region are calculated with the set parameters. In Practice it is not necessary for the lens whose potential and field are analytically obtained, for example, as in the Butler type.

(3) The electron trajectory is calculated as shown in Sec. 2-3.

(4) Then, the aberration coefficients are obtained from the axial potential and from the electron

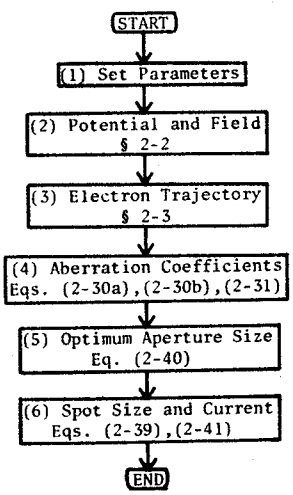

Fig. 2-8 Flow chart for computation of the lens characteristics.

trajectory by using the Eqs. (2-30a), (2-30b) and (2-31).

(5) When we want to obtain the minimum spot size, the optimum aperture size as shown in Eq. (2-40) should be calculated. If the aperture size is given as the input data, it is not necessary to calculate it.

(6) Then, the characteristics of the spot size, current and so on are all obtained.

It is very difficult to discuss the accuracy of the numerical calculation for the electron trajectories, aberrations and so on, because they are seldom calculated analytically. However, there is a desirable method. It is that the accuracy of the numerical calcuation for them is obtained in comparison with the values of Eq. (2-30a) and Eq. (2-30b), because they should be quite identical. For Butler type accelerating lens, the accuracies were checked by using the axial potential and from the electrode configurations. In the former the axial potential was obtained analytically, but in the latter the axial potential was obtained by using the mesh method as described in Sec. 2-2-1. The relative errors of the former were about 10^{-4}, 10^{-5}, 10^{-6} and 10^{-7} for the number of divisions of Simpson's 1/3 rule, N=20, 40, 50 and 100, in Eqs. (2-30a), (2-30b) and (2-31), respectively, under the conditions of S_0=3cm, L=2cm and V_0/V_1=7. The relative error of the latter was the order of 10^{-5} for N=100. These show that the lens characteristics can be sufficiently obtained by the numerical calculation. However, where the variation of the potential is large, for example, as the top of the tip of the field emission gun, it is difficult to obtain the accurate results of numerical calculations by using these numerical methods. In this model the variation of the potential more than $V_0/V_1=10^3 \sim 10^4$ leads to noticeable error, so it seems that this is upper limit in these numerical methods.

CHAPTER 3 BUTLER TYPE AND FLAT-PLATE ACCELERATING LENSES

§ 3-1 Introduction

The FE gun system has been the focus of attention of many researchers since Crewe's successful observation of single atoms (Crewe 1970). In his SEM he used the FE gun and an accelerating lens system of a particular configuration (Crewe 1966-1971). In designing this accelerating lens Butler (1966) tried to reduce the lens aberrations, and thus set the fiels at the apertures of the first and second anodes equal to zero. It was found that the minimum spherical aberration of the accelerating lens was associated with the axial potential.

$$\Phi(z) = P_3(z),$$

, in which P_3 was a cubic polynominal. By setting the fields at the apertures of the first and second anodes both to zero, it appears that the aperture effect of the anodes is neglected as will be described in Sec. 3-3. However, the quantitative comparison between Butler type and other simple lenses has not been reported so far as I know. Recently, the analysis of Butler type and flat-plate lenses was undertaken by Munro (1972) and Fraser et al (1971). Their estimation depends chiefly on the spherical aberration coefficient. But, from the author's computer simulation, the effect of chromatic aberration was much greater than spherical aberration. Therefore, the author tried to estimate the lens system by the spot size at the least confusion plane and by the current efficiency against Butler type and flat-plate lenses. In Sec. 3-2 the characteristics of these two lenses are described and in Sec. 3-3 the anode aperture effect which is very important to design and analysis is described. In Sec. 3-4 the comparison between the computer simulation data and the experimental results about the resolution in the flat-plate lens are described and the current efficiencies of these two lenses are described in computer simulation data and the experimental results. The comparison between these two lenses are summarized and discussed in Sec. 3-5.

§ 3-2 Characteristics of Butler type and flat-plate accelerating lenses

The models and the notations used in this analysis are shown in Fig. 3-1. The Butler type has the anode configuration corresponding to the following axial potential

$$\Phi(z) = 3z^2 - 2z^3 \quad . \qquad (3\text{-}1)$$

For the flat-plate lens the author has performed the calculation assuming that the thickness of the electrodes are infinitely small for simplicity of the calculation. Both the Butler type and flat-plate lenses have a circular aperture of 200 μm radius in the first and second anodes. The effect of this anode aperture was taken into consideration as described in Sec.3-3. The axial potential distribution was computed by using the mesh method, in which the space around the electrodes was divided into small section of 40μm. The lens characteristics described above are tabulated against the various voltage ratios V_0/V_1 for the position of the tip against the first anode, "S_0", in Table 3-1, where V_1 is taken as 3KV to calibrate the calculation of Crewe for the Butler type. Those values against S_0 = 1cm are particularly shown in Fig. 3-2. The conditions of these calculation were as follows: V_T = 0.2eV, ΔV = 0.2eV, R = 1000 Å and I_0 = 10μA. It is very difficult to manufacture this Butler type lens because of its particular anode configuration. When this type lens is reformed as shown

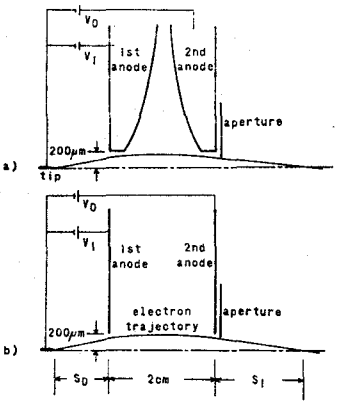

Fig. 3-1 Schematic diagram of the accelerating lens in the FE gun system. (a) and (b) are the Butler type and flat-plate accelerating lenses, respectively.

S_0(cm)	V_0/V_1	C_s(cm)	C_c(cm)	d(Å)	M	S_1(cm)	I(x10^{-11}A)	A_p(μm)
	3.0	1.463	1.502	64.2	1.01	-3.60	10.0	132
	5.0	2.368	3.865	103.	1.34	-4.77	6.6	82
	7.0	3.250	6.521	179.	2.12	-7.16	5.5	60
1.0	9.0	4.218	9.387	450.	5.05	-15.7	4.9	46
	11.0	5.279	12.43	1420.	-15.3	43.1	4.5	36
	13.0	6.422	15.65	302.	-3.14	7.92	4.2	29
	15.0	7.638	19.01	177.	-1.78	3.94	4.0	23
	3.0	7.649	3.704	127.	1.23	-5.74	4.1	110
	5.0	16.14	10.12	400.	3.23	-14.4	2.5	64
	7.0	26.29	17.79	628.	-4.51	18.2	2.0	43
2.0	9.0	38.08	26.43	203.	-1.35	4.71	1.7	31
	11.0	51.30	35.83	129.	-0.81	2.34	1.6	22
	13.0	65.78	46.07	97.5	-0.58	1.33	1.4	15
	15.0	81.39	56.95	80.3	-0.46	0.77	1.3	10
	3.0	26.41	6.910	211.	1.57	-9.08	2.2	99
	5.0	62.76	19.41	1370.	-7.95	42.9	1.3	55
	7.0	108.5	34.76	214.	-1.09	5.14	1.0	36
3.0	9.0	162.2	52.30	127.	-0.60	2.30	0.9	24
	11.0	223.9	71.75	94.2	-0.41	1.23	0.8	16
	13.0	291.4	92.89	77.0	-0.32	0.66	0.7	10
	15.0	364.6	115.6	66.3	-0.26	0.30	0.7	5

(a)

S_0(cm)	V_0/V_1	C_s(cm)	C_c(cm)	d(Å)	M	S_1(cm)	I(x10^{-11})	A_p(μm)
	3.0	8.262	1.155	76.3	0.94	-3.64	6.4	113
	5.0	11.30	3.053	103.	1.13	-4.33	5.5	80
	7.0	17.33	5.438	155	1.53	-5.47	4.4	57
1.0	9.0	26.81	8.308	281.	2.50	-8.00	3.6	40
	11.0	39.29	11.66	921.	7.53	-20.7	3.0	28
	13.0	54.35	15.50	931.	-7.06	15.9	2.5	20
	15.0	71.66	19.80	334.	-2.38	4.08	2.2	13
	3.0	45.75	3.018	138.	1.10	-5.44	2.7	94
	5.0	115.4	8.888	329.	2.06	-9.55	1.7	54
	7.0	233.2	16.97	13000	-68.9	273.	1.2	33
2.0	9.0	396.4	27.17	391.	-1.82	5.66	0.9	20
	11.0	600.0	39.46	215.	-0.91	1.93	0.8	11
	13.0	840.0	53.76	154.	-0.60	0.64	0.6	5
	15.0	1113.	70.02	123.	-0.45	-0.03	0.6	0.2
	3.0	178.4	5.814	233.	1.33	-7.99	1.4	81
	5.0	546.3	17.93	2710.	11.6	-63.2	0.8	43
	7.0	1153.	35.15	419.	-1.46	6.39	0.5	24
3.0	9.0	1982.	57.27	213.	-0.67	2.02	0.4	13
	11.0	3008.	84.13	151.	-0.43	0.64	0.3	5
	13.0	4215.	115.6	120.	-0.31	-0.04	0.3	4
	15.0	5585.	151.5	101.	-0.23	-0.45	0.3	5

(b)

Table 3-1 Characteristics of the Butler type (a) and flat-plate (b) accelerating lens with an anode aperture 400μm in diameter.

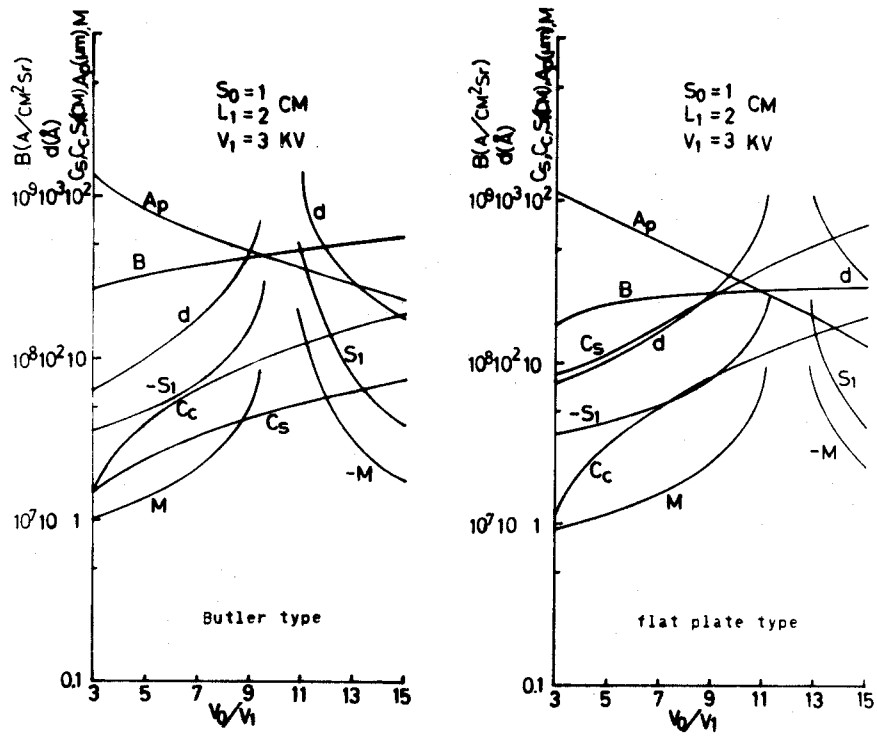

Fig. 3-2 Characteristics of the Butler type and flat-plate accelerating lens for S_0=1cm in Table 3-1.

in Fig.3-3, its chatacteristics changes as shown in Table 3-2. From tables 3-1 (a) and 3-2, it was found that the difference of C_s, C_c, M, S_1, d between the Butler type lens and its reformed lens were less than 10%.

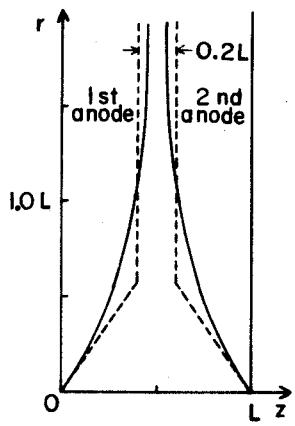

Fig. 3-3 Butler type lens shown by solid lines and its reformed lens shown by dotted lines.

S_0(cm)	V_0/V_1	C_s(cm)	C_c(cm)	d(Å)	M	S_1(cm)
	3.0	1.58	1.60	54.4	1.02	-3.66
	5.0	2.56	4.10	134.	1.41	-4.98
	7.0	3.36	6.86	318.	2.39	-7.96
1.0	9.0	4.18	9.78	1252.	7.39	-22.8
	11.0	5.12	12.86	1514.	-7.41	20.8
	13.0	5.90	16.08	608.	-2.55	6.38
	15.0	6.82	19.42	426.	-1.57	3.46
	3.0	8.14	3.90	106.	1.27	-5.90
	5.0	16.0	10.56	592.	3.89	-17.3
	7.0	24.6	18.36	746.	-3.41	13.7
2.0	9.0	33.8	27.0	342.	-1.22	4.22
	11.0	43.8	36.4	258.	-.754	2.18
	13.0	54.6	46.2	224.	-.554	1.28
	15.0	66.2	56.8	206.	-.443	.762
	3.0	27.4	7.26	189.	1.66	-9.54
	5.0	59.8	20.2	1088.	-5.17	27.6
	7.0	96.8	35.6	302.	-.997	4.64
5.0	9.0	158.4	55.0	222.	-.562	2.16
	11.0	184.4	72.0	192.	-.397	1.19
	13.0	251.0	92.4	177.	-.311	.660
	15.0	288.0	114.2	169.	-.258	.322

Table 3-2 Characteristics of the lens composed of the reformed anodes of the Butler type.

§ 3-3 Aperture effect of anodes

As described in Sec.3-2, many workers (Butler 1966, Munro 1972, Fraser et al 1971, Tonomura 1973) have studied on the accelerating lens. In their designs and analyses, however, the effect on the lens action of the aperture opened at the center of the anodes was seemed to be neglected and on this assumption the anode configuration and aberration coefficients have been calculated. But in actuality, as the anodes have limiting apertures where the electron beam passes through, the difference between the practical and theoretical potential of the neighbourhood of the apertures becomes a serious problem. So in this section, the result whether the aperture effect can be neglected is described. Tonomura (Tonomura 1973) also discussed the aberrations at the anode apertures and found to depend on the geometry of the electrodes. It seems that his results are coincident with my results . The model used for this is Butler type lens and is shown in Fig.3-4. The reason why both (a) and (b) in Fig.3-4, are investigated, is as follows. Namely, let assume that the point O represents the intersection of the Z axis and the designed anode configuration, r=f(z), and ℓ the distance between the point O and the plane of the anode, then ℓ equals to zero in (a) and $\ell \geq 10a_r$ in (b). The anodes actually manufactured are seemed in general to be situated between these two limiting models (a) and (b), that is, $10a_r > \ell > 0$. [The effect of the aperture in the case of $\ell \geq 10a_r$ agrees with that in model (b).] There are four types No.1, No.2, No.3 and No.4. No.1 and No.3 belong to (a), and No.2 and No.4 belong to (b).

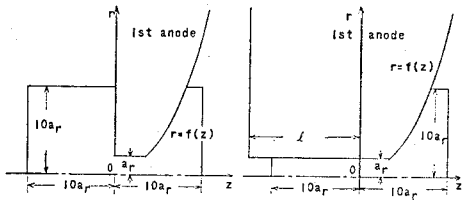

Fig. 3-4 Model used for the investigation of the aperture effect. a_r is the radius of the aperture opened at the center of the anode.

		C_s/L			C_c/L		
S_0/L	V_0/V_1	a_r=0.0	$N_0$1,2	$N_0$3,4	a_r=0.0	$N_0$1,2	$N_0$3,4
0.5	3.0	0.732	0.727	0.725	0.751	0.750	0.750
	5.0	1.184	1.175	1.175	1.933	1.927	1.929
	7.0	1.625	1.610	1.611	3.261	3.248	3.255
	9.0	2.109	2.086	2.088	4.694	4.673	4.686
	11.0	2.639	2.607	2.608	6.217	6.188	6.208
	13.0	3.211	3.168	3.167	7.823	7.785	7.813
	15.0	3.819	3.764	3.760	9.507	9.460	9.496
1.0	3.0	3.825	3.797	3.786	1.852	1.849	1.850
	5.0	8.069	7.990	7.968	5.060	5.044	5.050
	7.0	13.14	12.98	12.94	8.897	8.860	8.879
	9.0	19.04	18.77	18.69	13.21	13.15	13.19
	11.0	25.65	25.25	25.12	17.94	17.85	17.90
	13.0	32.89	32.33	32.14	23.04	22.91	22.99
	15.0	40.70	39.98	39.69	28.48	28.32	28.43
1.5	3.0	13.20	13.10	13.05	3.455	3.449	3.450
	5.0	31.38	31.04	30.91	9.705	9.672	9.685
	7.0	54.27	53.56	53.27	17.38	17.30	17.34
	9.0	81.32	80.11	79.59	26.15	26.02	26.09
	11.0	111.9	110.1	109.3	35.87	35.68	35.80
	13.0	145.7	143.2	141.9	46.45	46.19	46.35
	15.0	182.5	178.8	177.2	57.80	57.48	57.69

Table 3-3 Data for the test of the anode aperture effect. $N_0$1 and $N_0$2 have 100μm aperture, and $N_0$3 and $N_0$4 have 200μm.

No.1 and No.2 have an aperture of a_r = 100μm in radius, and a_r's of No.3 and No.4 are 200μm respectively. The models of the 2nd anode were considered in quite the same way. The mesh method was used to calculate the neighbouring potential of the aperture. To perform this calculation, it is necessary to know about the shape and size of the boundaries and also the potential along the boundaries. From some preliminary calculations it has become clear that it is enough to use $10a_r$ boundaries. In this way, the spherical and chromatic aberration coefficients (C_s and C_c) were obtained as shown in Table 3-3. The differences between the model (a) and (b) are enough little in numerical values and the data are summarized in Table 3-3. From these data, it is understood that the aperture effect can be neglected. Generally, C_s's with 100μm aperture are reduced less than 2%, and C_s's with 200μm aperture are reduced about 1 ∿ 3%, and C_c's with 100μm aperture and with 200μm aperture are reduced less than 1%. This reason is that the change of slope of potential is smaller than that in the cases when the aperture effect was neglected. From these, the method used by Crewe will be concluded to be right and the physical constants and the anode configuration can be calculated from the axial potential neglecting the effect of the anode apertures, so that it simplifies the analysis and design of the lens system.

In flat-plate lens, these results whether the aperture effect can be neglected could not be obtained. Because, when the axial potential which neglected the effect of the anode aperture are used, its field has the discontinuity at the points of anode apertures, so the physical constants of the lens can not be calculated accurately. Tonomura discussed that in the case of flat-plate lens the lens action is locally confined near the anode apertures and the spherical aberration at these points becomes about one hundredth of that for Butler type. From these reasons the characteristics of the flat-plate lens are obtained taking into consideration the anode aperture effect. The calculation procedure was the same as described above. The equipotential lines in the neighbourhood of the 1st anode aperture are shown in Fig. 3-5. The equipotential lines are normalized by the 1st and 2nd anode potentials which are regarded as zero and 1, respectively.

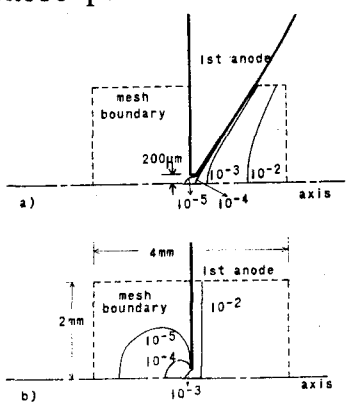

Fig. 3-5 Boundary conditions for (a) Butler type and (b) flat-plate.

§ 3-4 Comparisons between the computer simulation data and experimental results

As the detailed experimental results and their conditions of the operations in Butler type lens have not been reported, in this section the comparison between the computer simulation data and the experimental results of flat-plate lens is mainly described and the current efficiencies of the Butler type (Komoda's data, 1972) and flat-plate lens are described. A schematic diagram of the FESEM used is shown in Fig.3-6, and Fig.3-7.

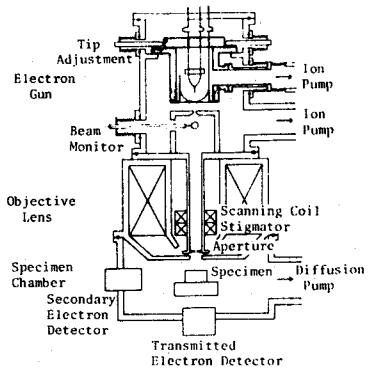

Fig. 3-6 Schematic construction of the FESEM.

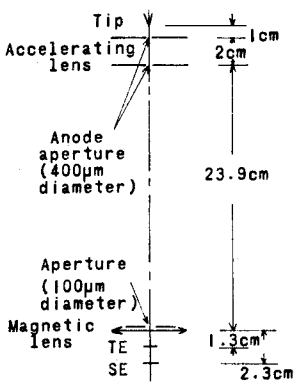

Fig. 3-7 Schematic diagram of the FESEM shown in Fig. 3-6.

This prototype FESEM was built by joint research between Osaka University and JEOL LTd. The image size of the FE gun and its accelerating lens demagnified with a mangetic lens can be calculated from the data of Table 3-1 or Fig.3-2 with the aberration coefficients, C_{sm} and C_{cm}, of magnetic lens whose aperture is 100μm in diameter. Magnetic lens characteristics such as C_{sm}, C_{cm}, focal length, convergence angle, demagnification and working distance are 80mm, 24mm, 21.2mm, 2.3×10^{-3} rad, 0.084 and 12mm for SE mode operation and 30mm, 13mm, 12.4mm, 3.8×10^{-3}rad, 0.046 and 2mm for TE mode, respectively. Hence one can calculate the ultimate image size d on a sample surface for practical conditions of operation from Eq.(2-47). In practice, since V_1 is 6.7 KV, and V_0 20KV for SE mode the ultimate resolution is theoretically calculated as 26.6 Å for the SE mode and as 15.5 Å for the TE mode at V_1=6KV and V_0=30KV, respectively. The resolution was experimentally estimated to be 20Å and 35 Å for TE mode and SE mode respectively. These are shown in Table 3-4.

As to the brightness, its degradiation by the accelerating lens and the auxiliary magnetic lens is as follows. In the Butler type the brightnesses of the electron source and on the specimen are 1×10^{9} and

mode	SE	TE
VI(KV)	6.7	6
VO(KV)	20	30
C_s(mm)	80	30
C_c(mm)	24	13
d_s(Å)	0.46	0.28
dc_s(Å)	4.1	8.5
dc_c(Å)	10.4	6.7
d_d(Å)	24.3	11.1
d(Å)	26.6	15.5
d_{exp}(Å)	35	20
M	0.08	0.05
f(cm)	2.12	1.24

Table 3-4 Characteristics for SE and TE mode operation.

BRIGHTNESS
(in SE Mode)

Data Source	Brightness (A/cm²str)		Degradiation
	Source	On the specimen	
T. Komoda and S. Saito, IITRI, SEM/ 1972, 129	1×10^9	7×10^7	0.07
Osaka Univ. and JEOL Ltd.	1×10^8	4.8×10^6	0.048

	Experiment	Calculation
Ratio of the degradiation	~1.5	~1.8

Table 3-5 Comparison between the Butler type and flat-plate accelerating lens in the degradation of the brightness.

7×10^7 A/cm^2·sr, respectively, from Komoda's data (Komoda et al. 1972). In the flat-plate lens they are 1×10^8 and 4.8×10^6, respectively. So as to the degradiation of the brightness the former is 0.07 and the latter is 0.048. Then, the ratio of the degradiation between the Butler type and flat-plate lens is experimentally obtained about 1.5. From the computer simulation result this ratio is about 1.8. These are shown in Table 3-5.

§ 3-5 Discussion and conclusion

From the Sec.3-2 ∿3-4 it was found that the computer simulation data were sufficiently reliable. And from Table 3-1 and Fig.3-2, it was found that, i) the spherical aberration coefficient C_s of the Butler-type lens is about one order of magnitude superior to that of the flat-plate one; ii) the chromatic aberration coefficient C_c of the Butler-type lens is a little superior in the range of large V_0/V_1, but is inferior to that of the flat-plate lens in the range of smaller V_0/V_1; iii) although the working distance S_1 must be considered when the spot size d is estimated, the spot size d of the Butler type is definitely superior to that of the flat-plate one in the range of larger V_0/V_1, but in the range of smaller V_0/V_1 it seems that there is no great differnce between them; iv) the beam current I of the Butler type is about two times larger than that of the flat-plate lens.

As mentioned above, the Butler type lens in the range of larger V_0/V_1 is definitely superior to the flat-plate lens. But, if the accelerating

lens is operated at a range of lower V_0/V_1, and particularly if an auxiliary magnetic lens is used in the focusing system, it seems that the Butler type has no greater advantages over the flat-plate type with respect to the spot size d. However the current efficiency (or degradation) of the Butler type is better than that of the flat-plate lens by about two times. The similar conclusions are obtained by Swann (1973), although it seems that his computer simulation results are based on the analysis of neglecting the anode aperture effect. It is described that the flat-plate accelerating lens has low aberrations and also this illuminating system is inherently brighter than that of Crewe type. However, it seems that this result is not confirmed experimentally. This reason seems to be that his analysis is based on the neglecting the anode aperture effect. Tonomura (1973) and Sec. 3-3 discuss that this effect can not be neglected for the flat-plate accelerating lens.

These arguments provide very useful data for the construction of FESEM with flat-plate anodes without encountering such difficulties as in the manufacture of the Butler type lens. Moreover, the above calculation show that FESEM, with this simple flat-plate lens system, is capable of achieving the resolution $\sim$ 35 Å in the SE mode, provided that the spatial diffusion of the secondary electrons in the specimen is of the same order of magnitude as the mean free path in the sample (Everhart et al. 1972). From these mentioned above, the author considered that the advantage of the Butler type lens consists in its higher current efficiency.

CHAPTER 4 NEW ACCELERATING LENS

§ 4-1 Introduction

The Butler type accelerating lens was designed to have a low aberration, particularly a small spherical aberration coefficient (Butler 1966). However, it seems that the merits of this type lens do not lie in its small spherical aberration but rather in its high current efficiency and lack of effect from the anode apertures as described in Chap. 3. The Butler type and other accelerating lens types which have been reported are almost composed of only two anodes. The optical properties of these lens systems are strongly dependent on the ratio of the field emission to accelerating voltages. So it is impossible to change the accelerating voltage for a fixed working distance without changing the given conditions (for example, the distance between the tip and the first anode, or changing the field emission voltage). When the accelerating voltage is changed, it seems that the working distance can be controlled by an auxiliary magnetic lens. However, changing the accelerating voltage over a wide range is very difficult because proper demagnification with the magnetic lens can not be obtained. To solve this problem, Plomp et al. (1968), Veneklasen and Siegel (1970 and 1972) proposed a method in which the first anode is replaced by an einzel lens. One of the parameters (for example, working distance) can be adjusted by means of the central anode of the lens for a given accelerating voltage. However, the accelerating lens system of this type becomes large in dimension and the aberrations also becomes larger in propotion to the dimension.

The author designed an accelerating lens system composed of three anodes. Someya et al. (1972 and 1974) suggested three anode accelerating lens, however, the anode configurations and the purpose are different from those of the present investigation. The lens system in the present investigation does not have the disadvantages of the above-mentioned systems and has the same or better characteristics. The lens are actually a hybrid of the immersion and unipotential lenses. This lens has also the great advantage by combining the auxiliary magnetic lens. Namely this lens can satisfactorily produce the optimum magnification for minimizing the spot size for the needed primary beam current and consequently the current efficiency of one order of magnitude higher than that of the accelerating lens composed of two anodes is obtained. These are shown in Sec. 4-5.

§ 4-2 Design of new accelerating lens

The spot size d was investigated by using the axial potential expanded in Fourier series

$$\Phi(z) = a_0 + b_0 z + \sum_{j=1}^{n} (a_j \cos jz\pi + b_j \sin jz\pi) \quad , \tag{4-1}$$

where $0 \leq z \leq 1$, and a_j and b_j are constants. This formula was nomalized to 1.0 for the axial separation of lenses with $V_1 = 0.0$ and $V_0 = 1.0$ for the voltages. The axial potential was expanded in Fourier series so that the off-axial potential could be analytically expressed by

$$\Phi(r,z) = a_0 + b_0 z + \sum_{j=1}^{n} a_j I_0(j\pi r)\cos jz\pi + \sum_{j=1}^{n} b_j I_0(j\pi r)\sin jz\pi \quad , \tag{4-2}$$

where I_0 is the zero-order modified Bessel function of the first kind. The optimum values of the constant a_j's, b_j's, and n can be automatically determined by an electronic computer. The NEAC 2200-model 700 computer was used to obtain the simulation data. The initial conditions and the symbols used were as follows: $V_T = 0.2$eV, $\Delta V = 0.2$eV, $R = 1000$Å, $V_1 = 5$KV, $I_s = 80\mu$A/sr. Thus, the lens system with the axial potential shown in Fig. 4-1 was obtained, with a spot size of about 1/15 that of the Butler type. Neglecting the difficulty of manufacture, we found from this calculation that (i) if the lens system is to have the axial potential shown in Fi. 4-1, it must have at least three anodes and (ii) when the lens system has only two anodes, the asymmetrical system of the first and second anodes as shown in Fig. 4-2(a) will

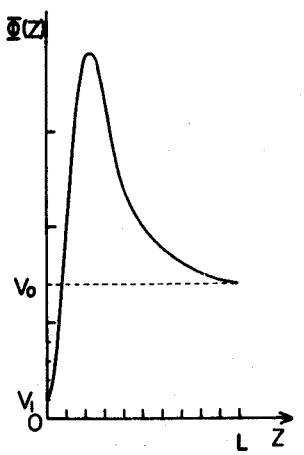

Fig. 4-1 Near-optimum axial potential for spot size d under the conditions of $V_0/V_1=7$ and $S_0/L=1.5$.

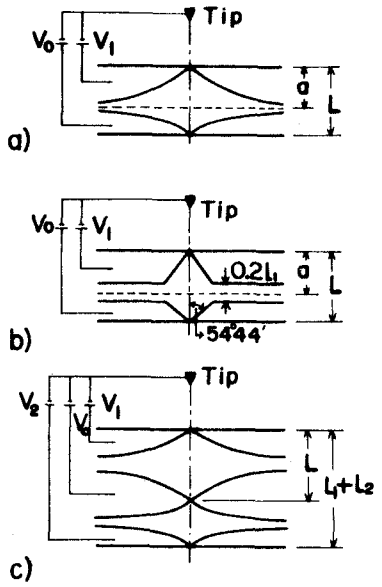

Fig. 4-2 Several models of the lens system:

(a) Asymmetric lens system, the shapes of first and second anodes are different from each other.

(b) Asymmetric lens system with reformed planes.

(c) Lens system with three anodes. In this lens system V_0 is the control voltage and V_2 is the accelerating voltage.

be better than the symmetrical one. With these results we tried to reduce the difficulty of actual manufacture by substituting the reformed plane anodes for the lens with curved surface such as the Butler type as described in Sec. 3-2. The author also tried to find whether it was possible to change the accelerating voltage without moving the working distance S_1, field-emission voltage V_1, etc. It was found that the substitution was possible by using reformed plane anodes such as those shown in Fig. 4-2(b). Change of the accelerating voltage was also found to be possible by adding a control anode as shown in Fig. 4-2(c). A computer simulation showed that the difference of C_s, C_c, M, S_1, d, etc. between the Butler-type lens and the reformed plane anodes as shown in Sec. 3-2 were less than 10 %. Therefore, the trial to analyze the following two lens models was performed: (I) the asymmetric and reformed plane lens with two anodes as shown in Fig. 4-2(b) and (II) the lens system with three anodes as shown in Fig. 4-2(c).

Although the author tried to improve the spot size of these lens system, it could not be done this very well in the range of accelerating voltages used by Crewe. Consequently, an accelerating lens system to be used in a lower range of accelerating voltages was tried. In

this voltage range the electron beam passing through the lens system generally diverges, if only two anodes are used as in Fig. 4-2(b). This suggests that three or more anodes are necessary to converge the electron beam in the lower range of accelerating voltages. So the characteristics of the accelerating lens system with three anodes were tried to investigate. The distance between the tip and the first anode was set $0.5L_1$ and the working distance S_1 was fixed at $2.5L_1$ and was controlled by V_0. The optimum value of V_0 was automatically determined by the Powell method (Powell 1964). With a view toward ease of actual manufacture, L_2 was taken equal to L_1. The characteristics of such lens systems, whose axial potential is expressed by third-, fifth-, and seventh-degree polynominals, are shown in Figs. 4-3(a) ∿4-3(c), respectively. The coefficients of third, fifth-,

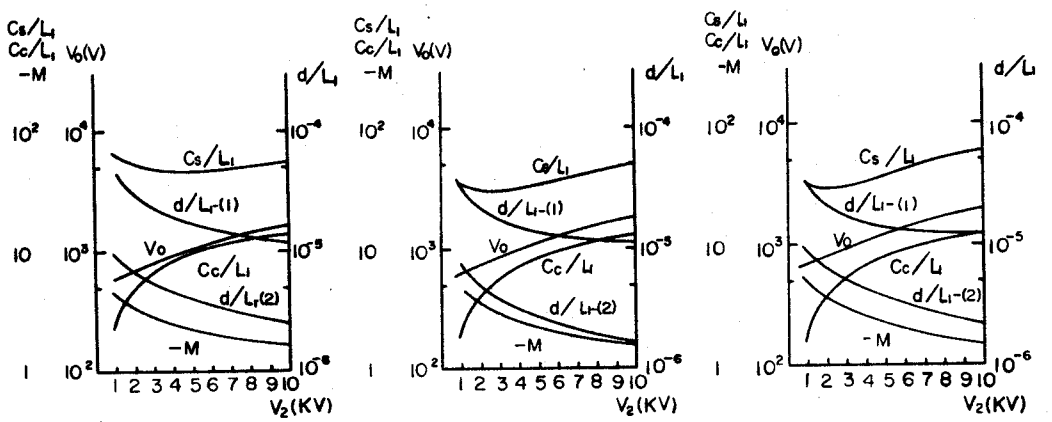

Fig. 4-3 Characteristics of the lens system with three anodes as shown in Fig. 4-2 (c). The axial potentials used are third-degree polynominal in (a), fifth-degree in (b), and seventh-degree in (c).

and seventh-degree polynominals were selected so that the first and higher derivatives would be equal to zero at each anode aperture. These lens system are shown in Fig. 4-4. (In Figs. 4-3, and 4-5, d/L_1-(1) is the spot size on the specimen corresponding to the beam current of 10^{-8}A, and d/L_1-(2) is the minimum spot size that can be obtained regardless of the beam current.) It was found from the data that the spot size d

on the specimen generally becomes smaller when higher-order polynominals are used for the axial potential. However, if higher-polynominals are used, there is a danger of producing a discharge because the distance between the anodes becomes too short. So, taking into consideration the discharge and the ease of actual manufacture, the author designed the lens system shown by the dotted lines in Fig. 4-4 as a substitute for the lens system using higher-order polynominals. Its characteristics are shown in Fig. 4-5 with $b = 0.2L_1$, and $\tan\beta = 0.8$. It was found that its characteristics are almost the same as those of the seventh-degree polynominal system except that C_s/L_1 is several percent smaller than for the latter shown in Fig. 4-5. If $b = 0.4L_1$, its characteristics are almost the same as those of the fifth-degree polynominal system and generally a few percent larger. This lens system is situated exactly between the fifth- and seventh-degree polynominals near the anode aperture, and this

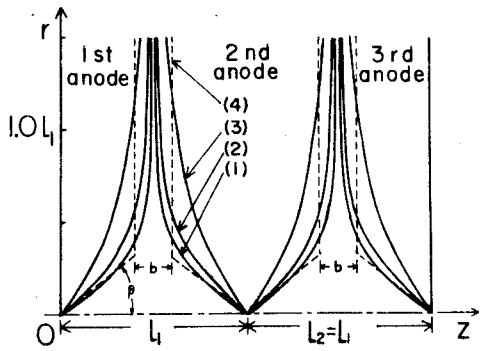

Fig. 4-4 Electrode configurations of the lens system with three anodes. Lines (1), (2) and (3) show the electrode configurations corresponding to the axial potentials expressed by seventh-, fifth- and third-degree polynominals. Line (4) shows reformed plane electrodes.

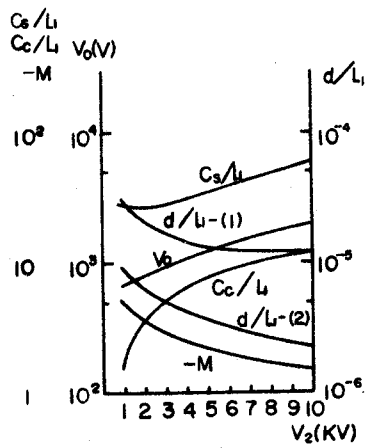

Fig. 4-5 Lens characteristics corresponding to the lens system shown by dotted lines in Fig. 4-4 with $b=0.2L_1$, $\tan\beta=0.8$, $S_0=0.5L_1$, $S_1=2.5L_1$ and $V_1=5$KV.

plays the most important part. It was also found that the lens characteristics depend on b, and that the smaller b is the better they are. Although the data are for low accelerating voltages, analogous data and advantages can also be obtained for higher accelerating voltages.

§ 4-3 Three anode accelerating lens

In the previous section the fundamental data about the design of a new accelerating lens are obtained. From these data the model of the new accelerating lens is determined as shown in Fig. 4-6. The configuration of the lens system indicated by the solid lines is expressed by the following axial potential,

$$\Phi(z) = (6z^5 - 15z^4 + 10z^3)(V_0 - V_1) + V_1 \qquad (4\text{-}3)$$

$$(0 \le z \le L_1 \ , \ L_1 = 2\text{cm}) \ ,$$

$$\Phi(z) = [6(z-L_1)^5 - 15(z-L_1)^4 + 10(z-L_1)^3](V_2 - V_0) + V_2 \qquad (4\text{-}4)$$

$$(L_1 \le z \le L_2 \ , \ L_1 = L_2 = 2\text{cm}) \ .$$

And the one indicated by the dotted lines correspond to tanβ = 0.8 and b = 1cm. The notations used are also in Fig. 4-6. Although the lens system indicated by the dotted lines in Fig. 4-6 is easier to manufacture than that shown by the solid lines, the latter is easier to work with in computer simulation than the former. Due to this, most of the data corresponds to the lens system of the

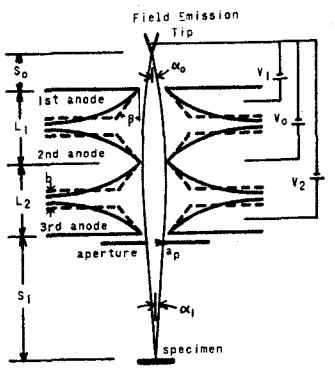

Fig. 4-6 Schematic diagram of the FE gun system with three anodes.

solid lines. The difference, however, between the data of these two models is not so large, as shown later.

§ 4-3-1 Relation between the working distance and its electron trajectory

In Sec. 4-2, only one electron trajectory was shown. However, it was found that there are generally two electron trajectories for a fixed working distance without a crossover point in the lens region. Some examples are shown in Fig. 4-7, and it can be seen that the appearance varies according to the voltages V_1, V_2, and V_0. Some specific examples are shown in Fig. 4-8, while their electron trajectories are shown in Fig. 4-9. In Fig. 4-9, two electron trajectories are different for the same V_1 and V_2, and thus, the minimum spot size d and the current efficiency of the electron beam are also different.

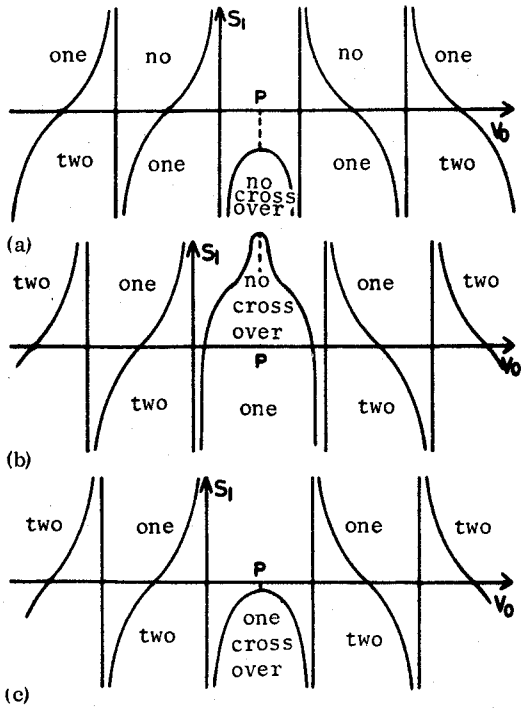

Fig. 4-7 Relation between the working distance S_1 and the control votage V_0 for some supplied field emission and accelerating voltages. The notations "no", "one", and "two" indicate the number of crossover point in the lens region.

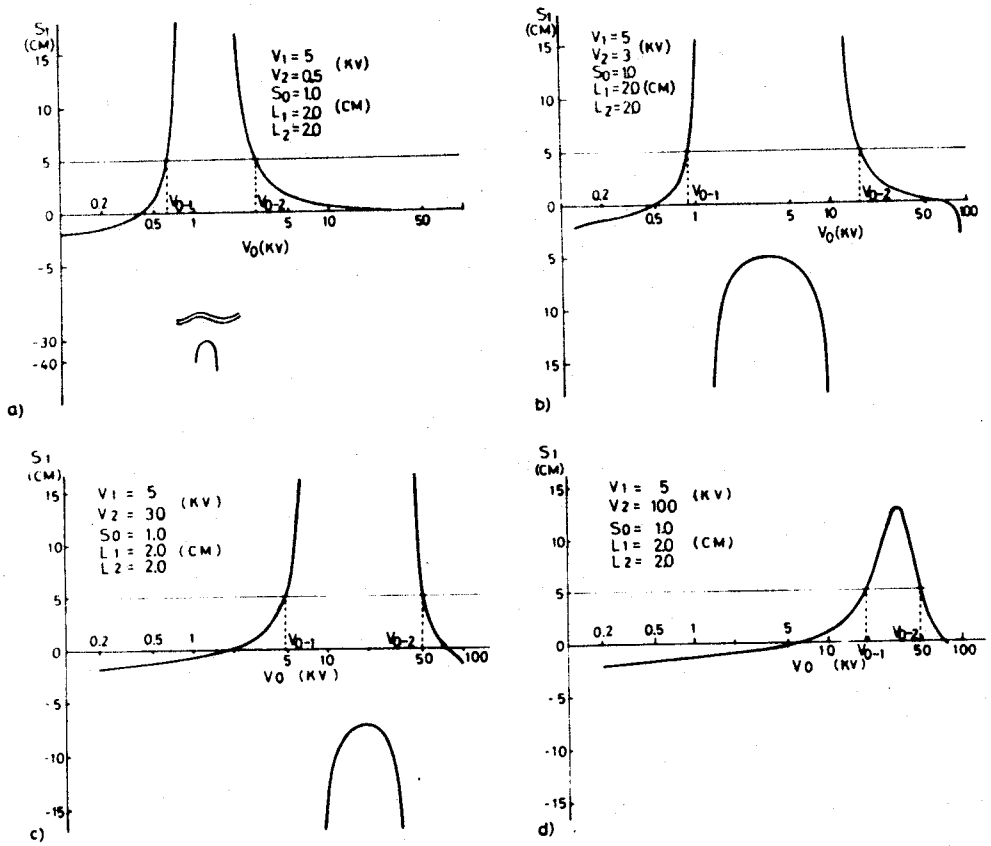

Fig. 4-8 Some specific example of Fig. 4-7.

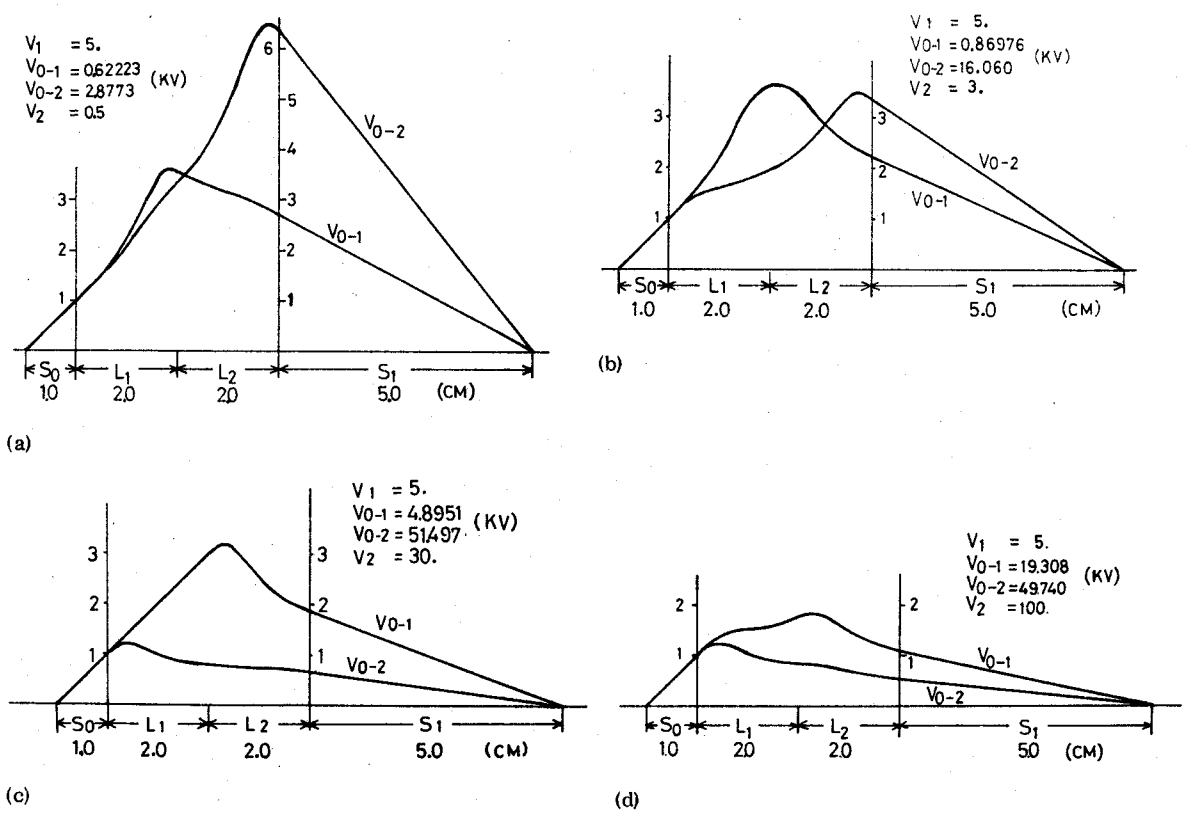

Fig. 4-9 Electron trajectories for fixed working distance.

§ 4-3-2 Principal characteristics

In the previous section, it was mentioned that there are two different V_0's and sets of characteristics for the same state. The characteristics for the following conditions are shown in Fig. 4-10: $L_1 = L_2 = 2cm$; $S_0 = 1,2cm$; $V_1 = 3,5KV$; $V_2 = 0.3 \sim 100KV$; $S_1 = 1.5, 5cm$; and $I_s = 30\mu A/sr.$; where L_1 and L_2 are the distances between the anodes, S_0 is the distance between the tip and the first anode, V_1 is the field emission voltage, V_2 is the accelerating voltage, S_1 is the fixed working distance and I_s is the emission beam current from the tip per steradian. We can reach the following conclusions from Fig. 4-10:

(1) Generally, there are V_{0-1} and V_{0-2} in V_0 for each given (V_1, V_2) and fixed working distance in a certain region of accelerating voltages. The difference between these values depends on V_2, but V_{0-1} and V_{0-2} are almost symmetrical to the point $V_2 = V_1$.

(2) The greater the working distance (the weaker the lens effect) is, the closer V_{0-1} and V_{0-2} are to the point $V_2 = V_1$.

(3) The difference between V_{0-1} and V_{0-2}, with $S_0 = 2cm$ for the fixed working distance, is smaller than that for $S_0 = 1cm$, because, if S_0 is larger, we can obtain the same working distance with a weaker lens effect. The point where V_{0-1} and V_{0-2} coincide corresponds to the point P in Fig. 4-7.

(4) The spot size d of V_{0-1} with the fixed working distance S_1 is larger than that of V_{0-2} for lower accelerating voltages, but the situation is reversed for higher accelerating voltages. The cross point exists approximately in the range of $V_2 = 10 \sim 20KV$ under the above conditions.

(5) The spot size d is generally smaller for higher accelerating voltages because the chromatic aberration and the diffraction effect are proportional to $1/\sqrt{V_2}$. However, the spot size d for V_{0-2} is a little reversed in the neighborhood of $V_2 = 5 \sim 20KV$, owing to the effect of the chromatic and spherical aberration coefficients.

(6) When an aperture is set under the third anode, the aperture size A_p which minimizes the spot size does not change appreciably if the accelerating voltage is changed from

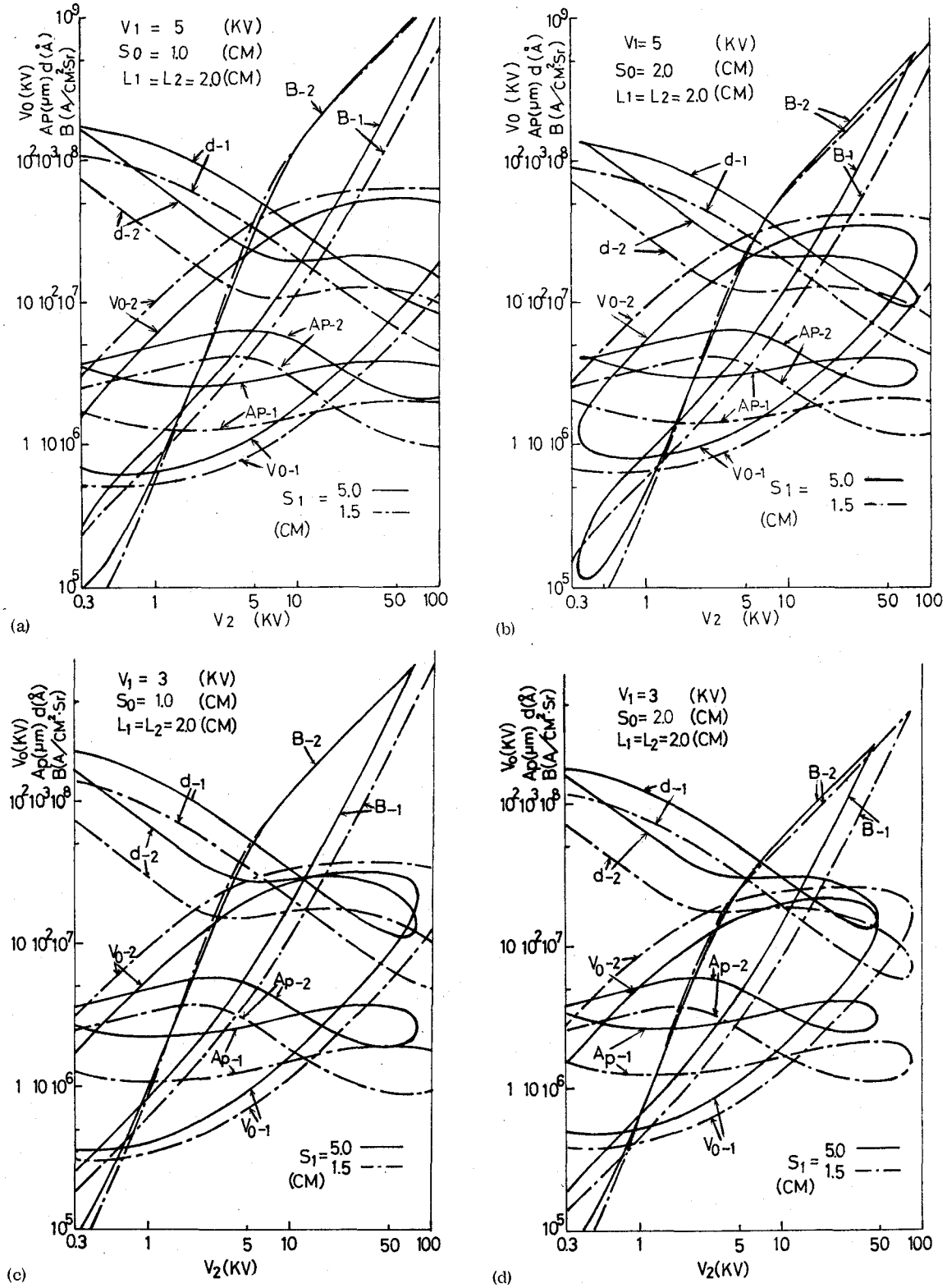

Fig. 4-10 Characteristics of the accelerating lens system with three anodes.

0.3KV to 100KV.

(7) The brightness B changes significantly as V_2 changes, and the difference between B_{-1} and B_{-2} reaches one order at maximum.

(8) As the paraxial ray equation is independent of the value of k in $k\phi\ (V_1, V_0, V_2)$, where k is a constant and ϕ is the axial potential of the lens region. Therefore, V_{0-1}'s (and V_{0-2}'s similarly) coincide when the graphs are overlaid to make the points of no lens effect coincident. For example, when the point corresponding to $V_1 = V_0 = V_2 = 5KV$ in Fig. 4-10(a) coincides with the point $V_1 = V_0 = V_2 = 3KV$ in Fig. 4-10(c), the control voltage plots also coincide. The control voltages for various other V_1's and V_2's can be predicted, and C_s, C_c and M can also be obtained in the same manner though they are omitted from Fig. 4-10. B, d and A_p, however, cannot be found in the same way.

§ 4-3-3 Experimental standpoint

In designing a SEM, various conditions and effects must be considered. This section discusses some simulation data from the experimental standpoint.

a) Configurations of the anodes

In Fig. 4-6 two anode configurations are shown. Since there is a danger of discharge if the anode configuration shown by the solid lines is used, an anode configuration corresponding to the dotted lines is substituted, where b = 1cm and $\tan\beta = 0.8$. It is clear the latter is easier to manufacture. The each value of the characteristics of the latter is less than that of the former by several per cent for V_0, about 2% for d, about 2% for A_p, and about 4% for B, under the conditions $V_1 = 5KV$, $S_0 = 1cm$, and $S_1 = 1.5$ and 5cm. The difference is small enough that we may conclude that it is sufficient to substitute the latter for the former.

b) Anode apertures

The effect of the anode apertures was ignored in the calculation of the characteristics of the accelerating lens system. However, when it is actually manufactured,

however, the anode aperture sizes must be determined, and their effect on the lens characteristics must be investigated. A criterion for deciding the anode aperture sizes is that all electrons that penetrate the first anode aperture should not collide with the second or third anode. For example, under the conditions $V_1 = 3 \sim 5KV$, $V_2 = 0.3 \sim 100KV$, $S_0 = 1 \sim 2cm$, $S_1 = 1.5 \sim 5cm$, the ratio of the first, second, and third anode apertures should be set at 1:7:7 if the fluctuation of 10% in V_0 is assumed. Although the effect of the anode apertures should be investigated, it is very difficult to calculate the lens characteristics as the function of the anode apertures by the mesh method when there are three anodes because of the problems associated with the boundary condition, calculation time, and accuracy. Instead, the author used another method for the calculation. In this method the lens characteristics can be calculated by using only the axial potential (refer to Chapter 2). The axial potential can be calculated from the following formula as the function of nonaxial potential (A. B. EL-Kareh and J. C. J. EL-Kareh, 1970):

$$\phi(0, z) = \tfrac{1}{2}\omega \int_{-\infty}^{\infty} \phi(1, \xi) \operatorname{sech}^2 \omega(z - \xi)\, d\xi, \qquad (4\text{-}5)$$

where $\omega = 1.31835$ and $\phi(1, \xi)$ is the nonaxial potential normalized to $r = P = 1$. P is the size of the anode aperture. The model used is shown in Fig. 4-11, and its specific formula is as follows.

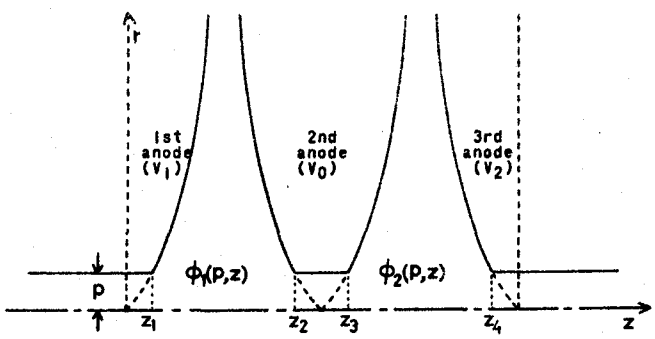

Fig. 4-11 Model for the investigation of the anode apertures. P is the size of the anode aperture.

Potential:

$$\begin{aligned}\phi(0,z) \approx & \tfrac{1}{2}V_1[1-\tanh\omega(z/P-z_1P)]+\tfrac{1}{2}\omega\int_{z_1/P}^{z_2/P}\phi_1(1,\xi)\\ & \times \operatorname{sech}^2\omega(z/P-\xi)\,d\xi\\ & -\tfrac{1}{2}V_0[\tanh\omega(z/P-z_3/P)-\tanh\omega(z/P-z_2/P)]\\ & +\tfrac{1}{2}\omega\int_{z_3/P}^{z_4/P}\phi_2(1,\xi)\operatorname{sech}^2\omega(z/P-\xi)\,d\xi\\ & +\tfrac{1}{2}V_2[1+\tanh\omega(z/P-z_4/P)].\end{aligned} \qquad (4\text{-}6)$$

The axial field can also be calculated analytically as a function of the axial potential from Eq. (4-6). The results for some anode aperture sizes are shown in Table 4-1. This table shows only the shift of the working distance. We may conclude from this table that it is better to keep the diameter of each anode aperture at less than 1 mm and to set them with the ratio of 1:7:7.

c) Optimum aperture size

The aperture sizes A_p in Fig. 4-10 are the optimum aperture sizes for the minimum spot size. The calculation procedure, however, is lacking in physical meaning. It is also difficult to change the aperture under the ultra-high vacuum condition. Therefore, the author investigated the effects due to a fixed aperture and the characteristics for the fixed aperture are shown in Fig. 4-12. From this figure it is found that the effects due to the fixed aperture size on the spot size and the brightness are small enough. The error from the optimum size may be less than 10%. Therefore, it seems that the effect of the aperture can be made small enough by dividing V_2 into groups and using the appropriate aperture for each group.

d) Tip

The distance S_0 between the tip and the first anode in Fig. 4-10 is of the order of 1 or 2cm, and the field emission voltage V_1 in Fig. 4-10 is assumed to be satisfactory for obtaining the necessary field emission current. S_0 and V_1 are sometimes different from those represented in Fig. 4-10 because of the tip conditions (for example, when the geometry of the tip is changed due to a bombardment by ions of residual gases). The effects of these S_0's and V_1's are shown in Table 4-2 and Fig. 4-13 for some sample accelerating voltages.

e) Stability of the electric power source

The author calculated V_0 so as the absolute accuracy of the working distance would be less than 0.001cm. When the supply voltages V_1, V_0, and V_2 fluctuate, the working distance shifts. The displacement of the working distance against the relative accuracy of the electric power source is shown in Table 4-3.

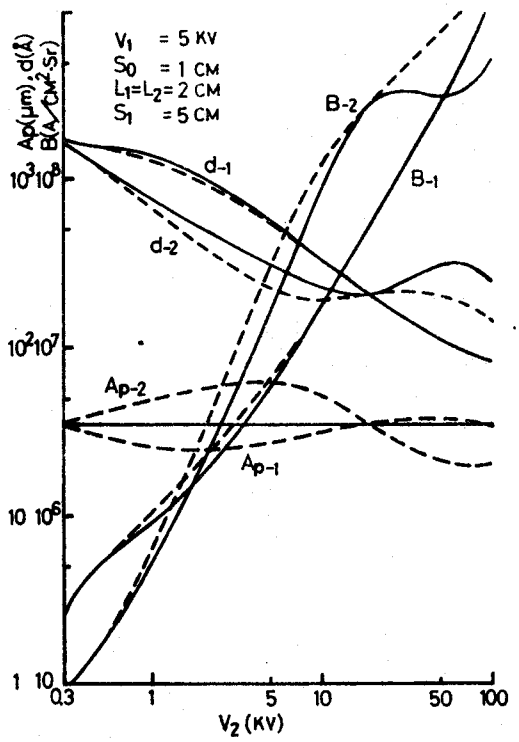

Fig. 4-12 Characteristics (solid lines) for a constant aperture size (35μm) set under the third anode. The characteristics of the dotted lines are for an optimum aperture size which minimizes the spot size.

V_2 (kV)	V_0 (kV)	Anode aperture (radius, mm) 0.0	0.2	0.5	1.0	
0.3	0.69619	4.999	4.999	4.993	4.987	
	1.5365	5.000	5.000	4.997	4.992	
3.0	0.86976	5.000	5.000	4.996	4.990	
	16.060	5.000	5.000	4.997	4.992	S_1 (cm)
20.	3.3153	5.000	5.000	4.996	4.990	
	47.688	5.000	4.998	4.991	4.975	
80.	14.370	5.000	4.999	4.995	4.989	
	52.270	5.000	4.998	4.986	4.968	

Table 4-1 The working distance for anode aperture sizes under the conditions V_1=5KV, S_1=1cm, and L_1=L_2=2cm.

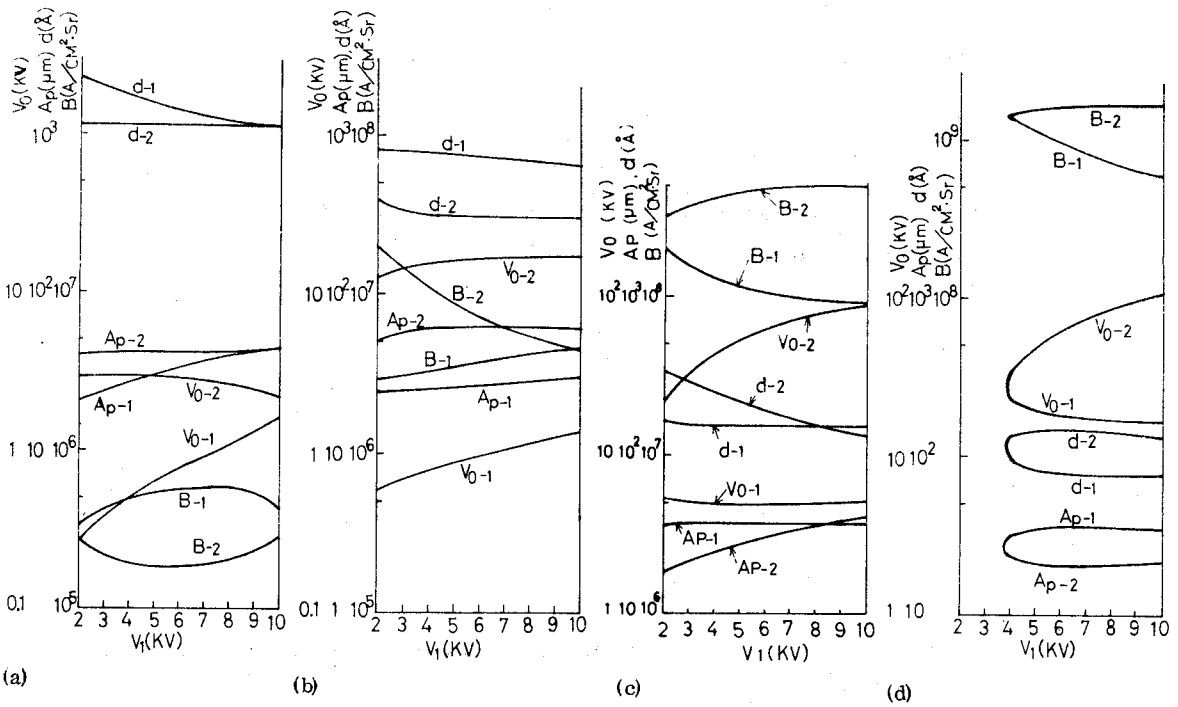

Fig. 4-13 Characteristics of sample conditions accompanying changes of the field emission voltage. (a) V_2=0.5KV, (b) V_2=3KV, (c) V_2=30KV, (d) V_2=100KV; S_0=1cm, L_1=L_2=2cm, S_1=5cm.

V_2 (kV)	S_0 (cm)	V_{0-1} (V)	V_{0-2} (V)
0.5	1.00	622.23	2877.3
	1.01	624.52	2871.7
	1.05	633.66	2856.2
	1.10	645.23	2835.1
3.0	1.00	869.76	16060.
	1.01	871.29	16034.
	1.05	879.76	15943.
	1.10	889.46	15805.
30.	1.00	4895.1	51497.
	1.01	4902.6	51202.
	1.05	4933.8	50073.
	1.10	4971.8	48733.
80.	1.00	14370.	52270.
	1.01	14409.	51875.
	1.05	14573.	50353.
	1.10	14770.	48568.

Table 4-2 Control voltage for the change of the distance between the tip and the first anode under the conditions V_1=5KV, S_1=5cm, and L_1=L_2=2cm.

V_2 (kV)		S_1 (cm) Relative error ×10^{-3}	×10^{-4}
0.5	V_{0-1}	4.938—5.063	4.994—5.006
	V_{0-2}	4.971—5.030	4.997—5.003
3.0	V_{0-1}	4.945—5.057	4.995—5.006
	V_{0-2}	4.967—5.034	4.996—5.004
30.	V_{0-1}	4.965—5.036	4.996—5.004
	V_{0-2}	4.929—5.074	4.994—5.008
80.	V_{0-1}	4.973—5.026	4.996—5.003
	V_{0-2}	4.933—5.067	4.993—5.006

Table 4-3 The working distance S_1 due to the fluctuation of the electric power source under the conditions V_1=5KV, S_0=1cm, and L_1=L_2=2cm. Relative error in this table is shown as the fluctuation of the electric power source.

§ 4-4 Comparisons between the electronic computer data and the experimental results

The comparisons between the electronic computer data and the experimental results of the characteristics of the three anode accelerating lens system for FESEM are described. Experimentally two characteristics were obtained. One of them is the relation between the accelerating voltages and the control voltages for the fixed working distance. The other is the variation of the current with the accelerating voltages.

Considering the easiness of manufacturing, this lens under test was designed as $L_1 = L_2 = 2cm$, $b = 1cm$, $\tan\beta = 0.8$, and the diameter of each of three anode apertures was 1mm in the lens indicated by the dashed lines. The specific structure in the vacuum chamber was as in Fig. 4-14 and the devices employed are shown in Fig. 4-15 and 4-16. This chamber was evacuated with an ion pump (160ℓ/s) down to the 10^{-10} torr region. The tungsten tip was operated without remolding processing.

Observing the luminescence from the fluorescence bombareded by the electron beam, the control voltage V_0 for the given physical constants (S_0, S_1, V_1, V_2 and so on) was adjusted by using the magnifier having a resolution of 7μm. It consists of the high resolution lens (Ultra-micro-Nichol with resolution 2μm) and the optical microscope, and it was set outside of the vacuum chamber. The distance between the tip and the first anode S_0 and the working distance S_1 are both freely changed

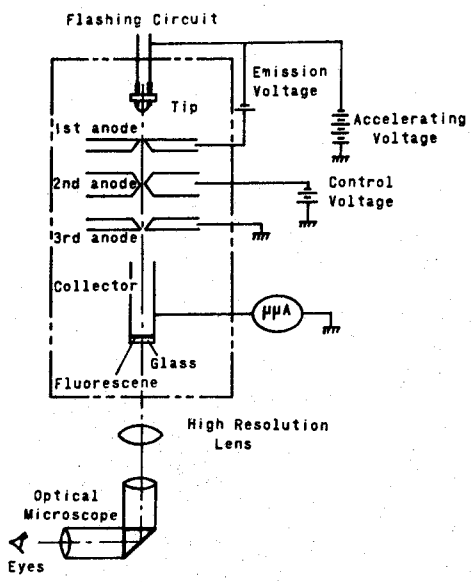

Fig. 4-15 Experimental device used for comparison with the computer simulation results.

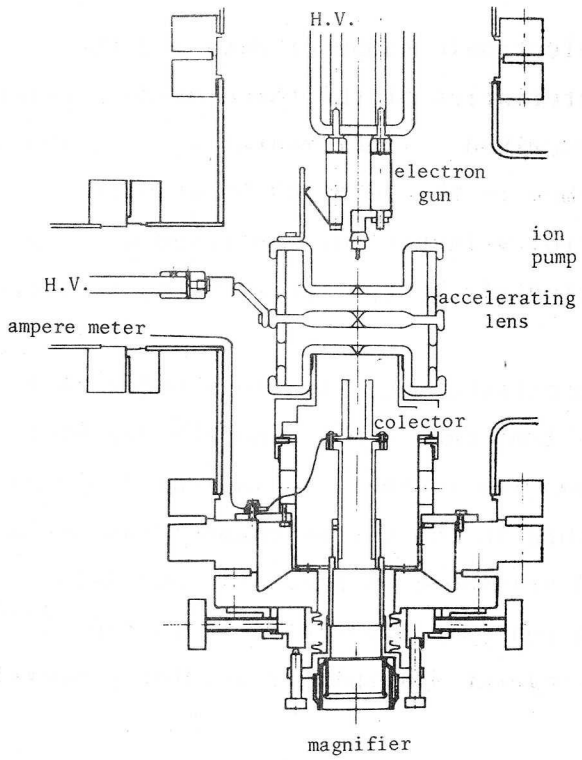

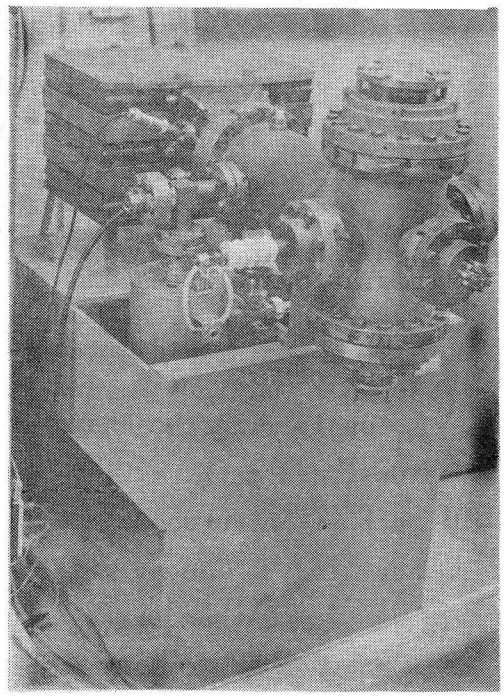

a) Vacuum chamber

Fig. 4-14 Specific diagram of the FE gun system in the chamber.

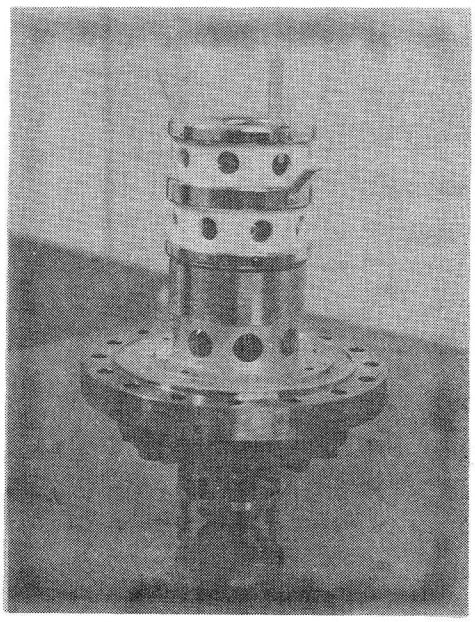

b) Three anode accelerating lens

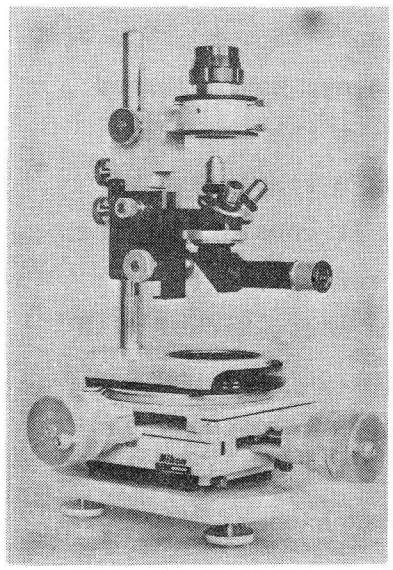

c) Magnifier

Fig. 4-16 Photographs of a) the vacuum chamber, b) the three anode accelerating lens and c) the magnifier.

by the bellows. As to the voltages, the data were normalized to V_1=3KV. The current per steradian (I_S) from the tip was also normalized to I_S = 30μA/sr. These experimental results and the computer simulation data are shown in Fig. 4-17. The accuracy of the measurement of the control voltage V_0 was about 2% and that of the current I was less than 7%. From Fig. 4-17 we found that the experimental values of V_0 coincide well with the computer simulation results, but the current I is about half of that in the computer simulation data. The difference is expected to be mainly due to the fact that neither the collector nor the electric wire was shielded and, to a small extent, due to the residual magnetization of the anodes, the charge up produced by the contamination in the neighbourhood of the anode apertures and so on. From the above results it was found that the computer simulation results were sufficiently reliable. It was also found that for the configurations of the anodes, there would be no significant difficulty though the author used the shape of the dashed lines in Fig. 4-6 was used instead of the conventional shape (for example, Butler type).

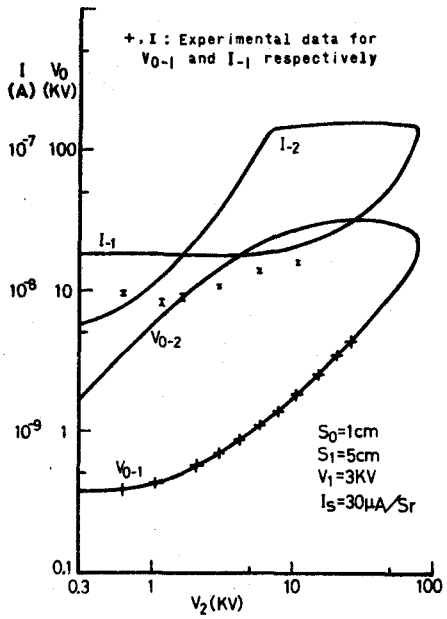

Fig. 4-17 Comparison between computer simulation and experimental results. V_0 is the control voltage for the fixed working distance and I is the current corresponding to the 1-mm-diam. anode aperture sizes.

§ 4-5 High current efficiency

The current efficiency of the lens system in case that the accelerating lens composed of three anodes is combined with an auxiliary magnetic lens in the FESEM is described.

The lens model used is shown in Fig. 4-18. The final spot size d on the specimen of this model will be expressed as follows [see Eq.(2-47)]:

$$d^2 = M_m^2(d_{Cs}^2 + d_{Cc}^2 + d_s^2) + d_{Csm}^2 + d_{Ccm}^2 + d_{dm}^2$$
$$= XM_w^2 + Y/M_w^2 + Z/M_w^6 \quad , \tag{4-7}$$

where M_w is the magnification of the whole lenses and X depends on d_{Cs}, d_{Cc}, d_s and d_{dm}, Y on d_{Ccm}, Z on d_{Ccm}. From Eq (4-7) it is expected that there is the optimum magnification M_w which minimizes the spot size d. However, the manification M_w must also satisfy the law of geometrical lens system,

$$M_w = (V_1/V_2)^{1/2}\alpha_0/\alpha_2 \quad . \tag{4-8}$$

In the accelerating lens composed of two anodes it is very difficult to obtain the optimum magnification of Eq. (4-7) which minimizes the d of Eq. (4-7) and also satisfies the condition (4-8) for the field emission and accelerating voltages, except for the particular condition. However, in the accelerating lens system composed of three anodes the magnification can be optimized easily, because, the working distance S_1 of the accelerating lens

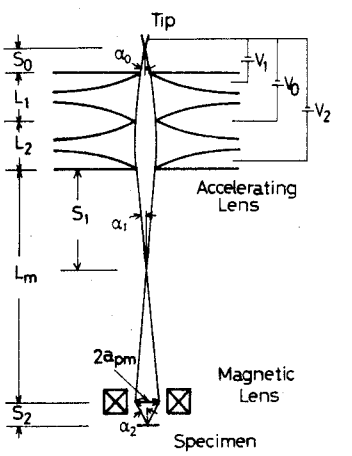

Fig. 4-18 The schematic diagram of the FESEM.

can freely be adjusted by the control voltage V_0 of the second anode as described in Sec. 4-3. This control voltage V_0 is not restricted by the other physical conditions and can easily be adjusted from the outside under the ultra high vacuum condition.

The characteristics of the relation between the spot size and the beam current are shown in Fig. 4-19 under the conditions of S_0 = 0.5cm, $L_1 = L_2$ = 2cm, I_s = 30μA/sr., R = 1000Å, V_1 = 3KV, V_2 = 25KV amd ΔV=0.2eV. Fig. 4-20 shows the optimum magnification M_w, limiting aperture size a_{pm} (in radius) and control voltage V_0 of the accelerating lens system composed of three anodes shown in Fig. 4-19. From Fig. 4-19, it is found that the current efficiency of the accelerating lens system composed of three anodes is one order higher than that of the accelerating lens composed of two anodes. And it should be noticed that the spot size represented by the dashed line in Fig. 4-19 for S_2 = 4 cm is considerably smaller than that for S_2 = 1cm in the higher beam current regions over about 1.7×10^{-10}A. This is due to the fact that the magnification in the case of S_2 = 4cm is nearer to the optimum magnification than that in the case of S_2 = 1cm.

The characteristics of this lens for the fixed beam current (10^{-7}A) on the specimen are shown in Fig. 4-21 for the accelerating voltages from 2KV up to 50KV. As shown in this figure the electron trajectory for the optimum magnification is abruptly changed at the certain accelerating voltage (∿13KV) for the conditions given in this

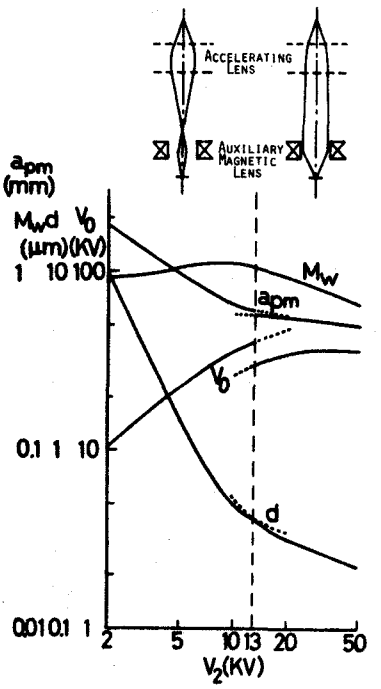

Fig. 4- 21 The characteristics for the fixed beam current (10^{-7}A) on the specimen under the conditions of S_0=0.5cm, C_{sm}=12cm, C_{cm}=5cm and S_2=4cm.

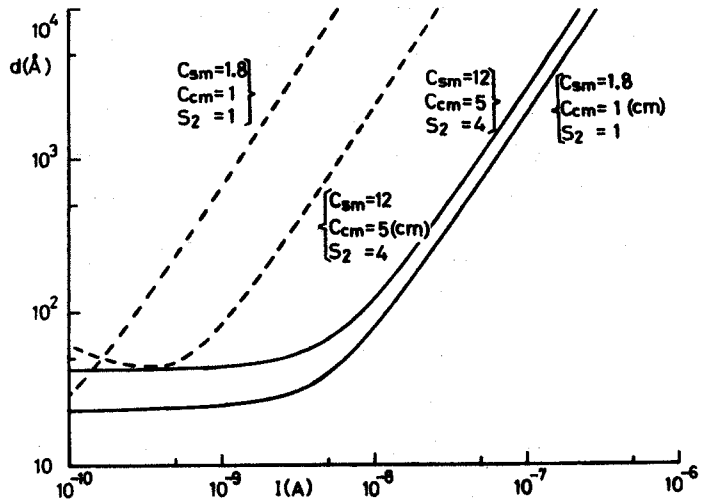

Fig, 4-19 The characteristics of the FESEM. The solid and dashed lines represent the characteristics of the accelerating lens composed of the three and two anodes, respectively, under the conditions of S_0=0.5cm, L_1=L_2=2cm, L_m=20cm, V_1=3KV, V_2=25KV and I_s=30μA/sr.. The units of C_{sm}, C_{cm}, and S_2 are centi-meter.

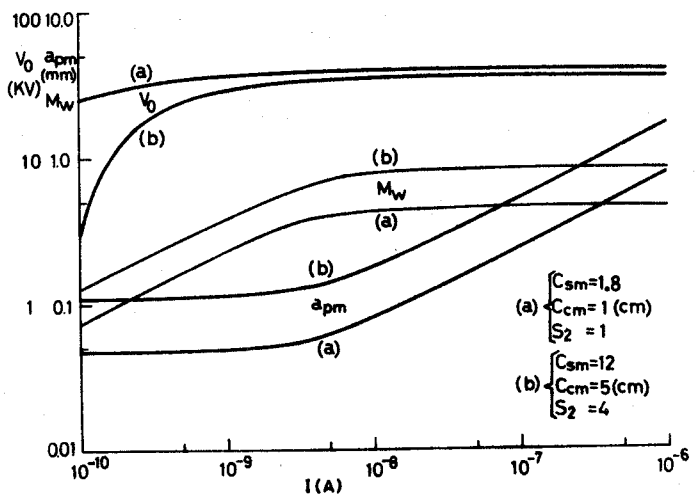

Fig. 4-20 The characteristics of the accelerating lens composed of three anodes shown in Fig. 4-19. The magnification M_w is the optimum value for the whole lens system. The units of C_{sm}, C_{cm} and S_2 are centi-meter.

calculation. Namely in the range of lower accelerating voltages (≤13KV) the electron beam trajectory corresponding to the optimum magnification has the crossover point, but that has no-crossover point in the range of higher accelerating voltage (≥13KV).

The shorter S_0 and L_m are, the smaller the spot size d for the fixed beam current is, but the change of the spot size by L_m is not so remarkable as that by S_0.

§ 4-6 Discussion and conclusion

The design and characteristics of the three anode accelerating lens have been described. The major advantages of this lens system are that the system can be used under various conditions by adjusting only the control voltage V_0 whether or not an auxiliary magnetic lens is used. Particularly it is noticeable that the lens system may be used over a wide range of accelerating voltages and the high beam current efficiency can be obtained for high beam current regions (more than about $10^{-9} \sim 10^{-8}$ Amperes).

The conventional accelerating lens is composed of two anodes. The optical properties of this lens is strongly dependent on the ratio of the emission and accelerating voltages. So it is very difficult to change the accelerating voltage over a wide range because proper demagnification with the magnetic lens can not be obtained. However, it is found to be possible by using the three anode accelerating lens because the optical properties can be adjusted by the control voltage.

It seems that the FE gun is at present inferior to the thermal electron gun on the point that the spot size becomes larger than that of the latter for high beam current regions (more than about $10^{-9} \sim 10^{-8}$ Amperes) (Broers 1972, see Fig. 1-4). The reason of this seems to be as follows. In the low beam current regions (less than 10^{-9} Amperes) the limiting aperture size is small. Then the spherical aberration of the accelerating lens can be reduced enough small by the demagnification effect of the auxiliary magnetic lens. However, it becomes to play a major role for high beam current regions (the large limiting aperture size). So if we would try to obtain the smaller spot size in the high

beam current region, the accelerating lens with smaller spherical aberration must be designed. This is very difficult because the spherical aberration is increased in propotion to the third power of the limiting aperture size. However, there are methods which overcome this difficulty. The one of the approaches is to use the optimum magnification for the given physical conditions (for example, the field emission voltage, the accelerating voltage, the emission current and the beam current) as described in Sec. 4-5. As for the accelerating lens composed of two anodes, the magnification produced by the whole lens system with this lens is physically restricted and cannot be controled easily. Namely the difference between the magnification of the whole lens and the optimum magnification becomes larger when the high beam current is requested. The three anode accelerating lens is suitable for this purpose because the whole lens system can be operated under the optimum condition. This fact is due to that the optical properties can be adjusted only by the control voltage. Consequently we can obtain the current efficiency which is one order higher than that of the two anode accelerating lens.

Thus, the three anode accelerating lens has remarkable advantages. The similar results are obtained by using the preaccelerator lens (einzel lens)and accelerator proposed by Veneklasen (1972), although only the spherical aberrations of the preaccelerator lens and magnetic lens are considered. Someya et al. (1972 and 1974) proposed the three anode accelerating lens, but the anode configurations are quite different from that of the present investigation and also this lens is designed to eliminated the damage to the field emitter due to discharges in the gun chamber.

It was also found that for the configurations of the anodes there would be no significant difficulty even though we used the shape of the dashed lines in Fig. 4-6 instead of the curved shape (for example, the Butler type).

From above fact, it seems that not only in the field of conventional SEM but also in the field of investigations such as Scanning Auger Electron Microscope (MacDonald 1970 and 1971), Electron Beam Microfabrication (for example, Brewer 1971, Broers 1972 and Angello 1973) and so on the FE gun system consisted of the three anode accelerating lens is expected to become a powerful tool in future.

CHAPTER 5 SOME OTHER COMPUTER SIMULATIONS

The electron optical properties of the accelerating lens of FESEM have been mainly analyzed until Chapter 4. However, these are some points which are lacking in physical substances or based on an over-simplified and unrealistic model. So in this chapter some points which can be easily analyzed by computer simulation are described.

In Sec. 5-1, the electron trajectories emerging from the tip and the virtual source size of the tip as an electron source are discussed. In Sec. 5-2, the intensity distribution of the electron beam on the specimen is computed by using the pupil function in terms of the electron wave optics, and the spot size (defined as 80% of the total electron beam spread) is precisely obtained from this intensity distribution. In Sec. 5-3, the influence of the eccentricity of electrostatic lenses on the spot size is analytically formulated and is numerically calculated for the Butler type and the three anode accelerating lens.

§ 5-1 Electron trajectory and virtual source of FE gun of SEM

§ 5-1-1 Introduction

It is very important to know the electron trajectories emitted from the tip and a virtual source size of the tip for electron optical design, yet these calculations for pointed cathodes have been based on an oversimplified and unrealistic model, that is a spherical emitter concentric with a spherical anode.

Generally speaking, the field emission tip has the dimension of the order of 1000Å and the distance between the tip and the anode is the order of centimeters. This large difference of dimensions makes it quite difficult to analyze accurately the potential and the field between them. So the author tried to analyze them using a particular model, that is a sphere-on-orthogonal-cone model (SOC model) suggested by Dyke et al.(1953), which seems to be much better model than the simple spherical model. Wiesner and Everhart (1970 and 1973) have already analyzed in detail the electron optical properties of this electron source by using the SOC model. The calculations in this section are performed for the purposes of the confirmations of the Wiesner's results and of the validity of Eq. (2-37). It is noted that this model doesn't seem to be applied to the tip of the remolding processing, because this processing will bring a special shape of the tip.

§ 5-1-2 Potential and field analyses

This SOC model and its notations are shown in Fig. 5-1. The SOC model is known as the core of the system. The potential (ϕ) and fields (E_ρ, E_θ) of this system in spherical coordinates (ρ, θ, ψ):

$$\phi(\rho,\theta) = k \frac{V_1}{S_0^n} \left(\rho^n - \frac{a^{2n+1}}{\rho^{n+1}}\right) F(-n,\ 1+n,\ 1,\ (1-\cos\theta)/2) - V_{00} \quad , \tag{5-1}$$

$$\begin{aligned} E_\rho &= - \frac{\partial\phi(\rho,\theta)}{\partial\rho} \\ &= - k\ (V_1/a)\ (a/S_0)^n \left\{ n\,(a/\rho)^{1-n} + (1+n)(a/\rho)^{2+n} \right\} \\ &\qquad \times F(-n,\ 1+n,\ 1,\ (1-\cos\theta)/2) \quad , \end{aligned} \tag{5-2}$$

$$\begin{aligned} E_\theta &= - \frac{1}{\rho} \frac{\partial\phi(\rho,\theta)}{\partial\theta} \\ &= kV_1/\rho\ (a/S_0)^n \left\{ (\rho/a)^n - (a/\rho)^{n+1} \right\} n(n+1)/2\ \sin\theta \\ &\qquad \times F(1-n,\ 2+n,\ a,\ (1-\cos\theta)/2) \quad , \end{aligned} \tag{5-3}$$

where a is the radius of the core sphere, ρ is the distance from the center of sphere, ρ_0 is the radius of the tip curvature, k and V_{00} are determined by the next Eqs. (5-4) and (5-5),

$$\phi(\rho_0,\ 0) = 0 \quad , \tag{5-4}$$

$$\phi(S_0,\ 0) = V_1 \quad , \tag{5-5}$$

and the constant n is determined by the reqirement that the hypergeometric function F[-n, 1+n, 1, (1-cosα)/2] equals to zero, where α is the exterior half-angle of the cone, as shown in Fig. 5-1. n and ρ_0/a are called the cone index and form

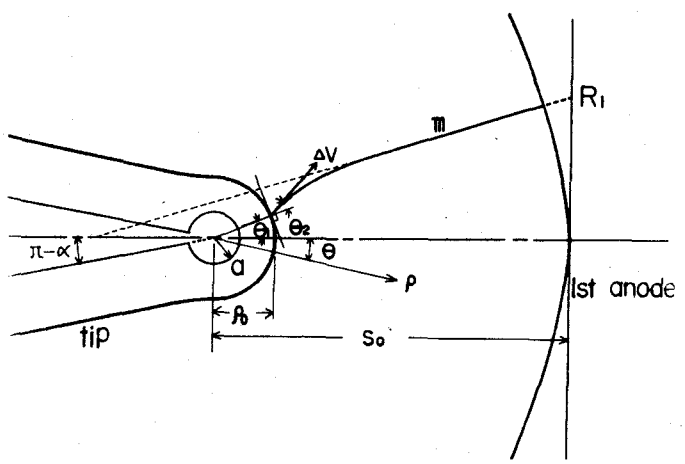

Fig. 5-1 The schematic diagram between the tip and the anode. The tip was represented as an equipotential surface of a sphere-on-orthogonal cone.

ratio respectively and decided from the tip configuration and thereby the anode configuration is uniquely decided. This is because that the range in which the value of constant n can actually take is limited merely from 0.1 to 0.2 and in this range the change of the tip configuration is small, thereby the change of anode configuration is also small. Hence it seems sufficient to calculate the trajectory only for the typical model of the tip so long as we consider merely the electron trajectories located very near to the optical axis.

§ 5-1-3 Analysis of the electron trajectory

The electron trajectories between the tip and the 1st anode can be obtained by using the next equations in cylindrical coordinates

$$\frac{d^2r}{dt^2} = -\eta E_r \quad , \tag{5-6}$$

$$\frac{d^2z}{dt^2} = -\eta E_z \quad , \tag{5-7}$$

where, η is the magnitude of the electronic charge-to-mass ratio and t is the time. E_r and E_z are expressed in terms of E_ρ and E_θ of Eqs. (5-2) and (5-3) by (see Fig. 5-2)

$$E_r = E_\rho \sin\theta + E_\theta \cos\theta \quad , \tag{5-8}$$

$$E_z = E_\rho \cos\theta - E_\theta \sin\theta \quad . \tag{5-9}$$

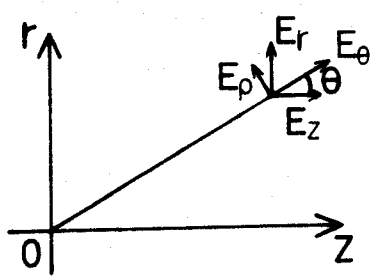

Fig. 5-2 Force vector by electric field at (r,z).

Here, when we numerically calculate the electron trajectories by using these equations, we cannot use Runge-Kutta method as described in Sec. 2-3 because of the high field ($>10^7$ volt/cm) at the top of the tip. So the author used the predictor-corrector method (especially, Hamming method) in order to calculate accurately and shorten the calculation time. This method is as follows. Let the equations to be solved are

$$dy_i/dx = f_i(x, y_1, y_2, \ldots\ldots, y_n) \quad , \tag{5-10}$$

where i = 1, 2, 3, ..., n,

x is the independent variable and y_1's are the dependent variable. In Hamming method, the following formulae are used, assuming the solution has been completed through the k^{th} step the quantities are to be understood as vectors with dimension equal to the number of equations to be integrated. The subscripts k, k+1 refer to quantities evaluated at the k^{th} and $k+1^{th}$ steps, respectively.

Predictor

$$P_{k+1} = y_{k-3} + 4/3h(2y'_k - y'_{k-1} + 2y'_{k-2}) \tag{5-11}$$

Modifier

$$M_{k+1} = P_{k+1} - 112/121(P_k - C_k) \tag{5-12}$$

$$M'_{k+1} = f(x_{k+1}, M_{k+1}) \tag{5-13}$$

Corrector

$$C_{k+1} = 1/8[9y_k - y_{k-2} + 3h(M'_{k+1} + 2y'_k - y'_{k-1})] \tag{5-14}$$

Final Value

$$y_{k+1} = C_{k+1} + 9/121(P_{k+1} - C_{k+1}) \tag{5-15}$$

where, h is the step size. In order to calculate according to the above procedure, Runge-Kutta method is used for the values of the initial four steps because they must be known as shown in Eq. (5-11). Hamming method is used after these initial four steps and this calculation procedure is shown in Fig. 5-3. Eqs. (5-6) and (5-7) are transformed as follows,

$$dr/dt = V_r \quad ,$$

$$dV_r/dt = - E_r \quad , \tag{5-16}$$

$$dz/dt = V_z \quad ,$$

$$dV_z/dt = - E_z \quad ,$$

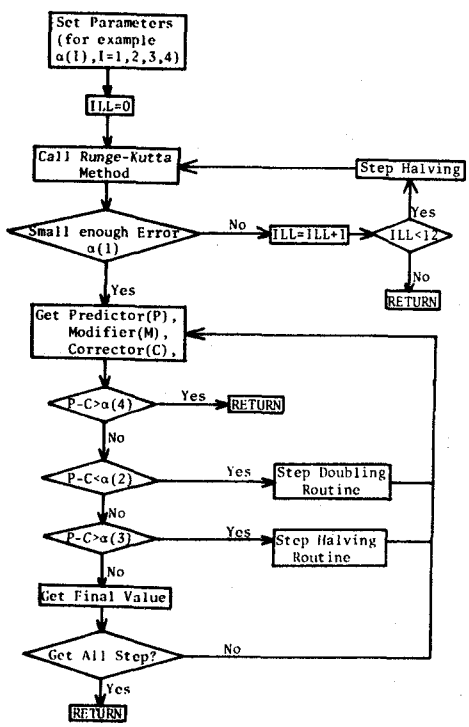

Fig. 5-3 Flow-chart of Hamming method.

and these equations are numerically solved by using the Hamming method.

§ 5-1-4 Simulation data and discussion

By using the theory and calculation procedure as described in Secs. 5-1-2 and 5-1-3, the electron trajectories between the tip and the anode can be analyzed. Here, the tip and anode configurations were analyzed for n = 0.15 (α = 175°48') and ρ_0/a = 2.0 which give the typical tip configuration which Wiesner (1970 and 1973) used. Then, the tip and anode configurations are shown in Figs. 5-4 and 5-5. In this investigation the trajectories for three groups of electrons as shown in

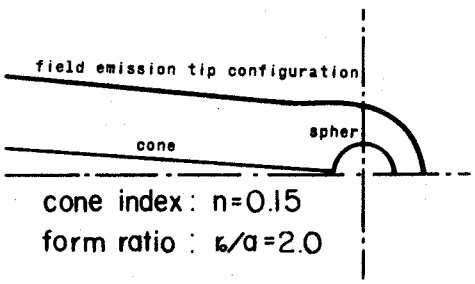

Fig. 5-4 Typical cathode shape with core.

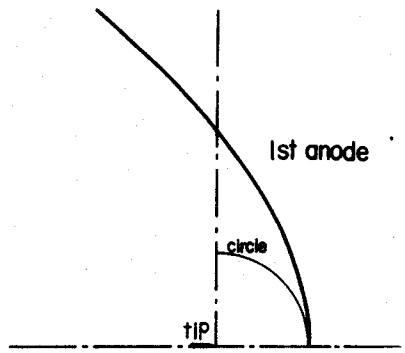

Fig. 5-5 Typical anode shape for the cathode with (n, r_0/a) = (0.15, 2.0).

Table 5-1 were calculated and these results are shown in Tables 5-2, 5-3 and 5-4. These data are represented quite satisfactory by the following formulae.

In Tabel 5-2,

$$R_1 = (5433553 - 3330\ \Delta V)(\Delta V)^{1/2} \times 10^{-8}\ \text{cm} \quad , \qquad (5\text{-}17)$$

$$m = (5175636 - 3630\ \Delta V)(\Delta V)^{1/2} \times 10^{-8} \quad , \qquad (5\text{-}18)$$

in Table 5-3,

$$R_1 = (8562217 + 3\theta_1 + 39\theta_1^2)\theta_1 \times 10^{-9}\ \text{cm} \quad , \qquad (5\text{-}19)$$

$$m = (8155730 + 3\theta_1 + 150\theta_1^2)\theta_1 \times 10^{-9} \quad , \qquad (5\text{-}20)$$

and in Table 5-4

$$R_1 = (581677 + \theta_2 - 27\theta_2^2)\theta_2 \times 10^{-9} \text{ cm} \quad , \tag{5-21}$$

$$m = (554073 - 0.5\theta_2 - 25.5\theta_2^2)\theta_2 \times 10^{-9} \quad , \tag{5-22}$$

If this study is improved more in detail and the more accurate values of constants and coefficients of each equations are obtained, we will be able to know the position and inclination of the trajectories on the anode easily without examining the electron trajectories. And also we will be able to get information about the virtual source using the appropriate weight for each initial condition. Now, the radius of a virtual source is about 30Å for $\Delta V = 0.0 \sim 0.4$ eV with the same weight, one. Practically, however, θ_2 of the electron leaving the tip is very small, so, for example, the virtual source size were about 0.25Å for $\theta_1 = 0°$, $\Delta V = 0.4$ eV, $\theta_2 = 0 \sim 10°$. From these results, it seems that the Eq. (2-37) is a little overestimated, but it will be sufficient to use Eq. (2-37) for the calculation of the virtual source size from the standpoints of the easiness of the calculation and the calculation time.

Group	θ_1	θ_2	ΔV
(1)	0	$\pi/2$	various
(2)	various	0	0
(3)	0	various	0.4eV

Table 5-1 Initial conditions

	R_1 ($\times 10^{-2}$cm)		m ($\times 10^{-2}$cm)	
θ_2	computer	(5-21)	computer	(5-22)
1°	0.581651	0.581651	0.554047	0.554047
2°	1.163143	1.163142	1.107940	1.107940
3°	1.744311	1.744311	1.661526	1.661526
4°	2.324995	2.324997	2.214650	2.214652
5°	2.905034	2.905034	2.767161	2.767165
6°	3.484267	3.484266	3.318903	3.318912
7°	4.062530	4.062529	3.869721	3.869740
8°	4.639668	4.639656	4.419467	4.419496
9°	5.215519	5.215491	4.967985	4.968027
10°	5.789922	5.789870	5.515125	5.515180

Table 5-4 The computation data and the values by Eqs. (5-21) and (5-22), whose initial conditions are θ_1=0, ΔV=0.4eV.

	R_1 ($\times 10^{-2}$cm)		m ($\times 10^{-2}$cm)	
ΔV(ev)	computer	(5-17)	computer	(5-18)
0.001	0.1718239	0.1718239	0.1636679	0.1636679
0.005	0.3842091	0.3842091	0.3659715	0.3659715
0.01	0.5433520	0.5433520	0.5175601	0.5175600
0.05	1.2149423	1.2149422	1.1572668	1.1572668
0.1	1.7181351	1.7181350	1.6365648	1.6365650
0.2	2.4296610	2.4296610	2.3142896	2.3142901
0.3	2.9755325	2.9755324	2.8342152	2.8342161
0.4	3.4356384	3.4356382	3.2724402	3.2724413

Table 5-2 The computation data and the values by Eqs. (5-17) and (5-18), whose initial conditions are θ_1=0, θ_2=π/2.

	R_1 ($\times 10^{-2}$cm)		m ($\times 10^{-2}$cm)	
θ_1	computer	(5-19)	computer	(5-20)
1°	0.8562259	0.8562259	0.8155748	0.8155748
2°	1.7124758	1.7124758	1.6311592	1.6311592
3°	2.5687730	2.5687730	2.4467621	2.4467622
4°	3.4251408	3.4251412	3.2623929	3.2623929
5°	4.2816026	4.2816035	4.0780604	4.0780600
6°	5.1381810	5.1381834	4.8937728	4.8937728

Table 5-3 The computation data and the values by Eqs. (5-19) and (5-20), whose initial conditions are θ_2=0, ΔV=0eV.

§ 5-2 Determination of the spot size by using the intensity distribution

The intensity distribution on the specimen was computed by using the pupil function in terms of electron wave optics, and the spot size (80 % of the total electron beam spread) was precisely obtained from this intensity distribution. From the computer simulation data the following results were obtained. (1) The spot size determined by the conventional method was generally over-estimated. (2) The difference in the optimum aperture size determined by the conventional method and by the electron wave optical method was of very small order of magnitude.

§ 5-2-1 Introduction

In the lens design, it is very important to estimate the resolving power produced by the lens defect. In this design, the electron beam spread (spot size) d on the specimen has usually been defined by Eq. (2-39) in Sec. 2-4. However it seems that this definition is rather poor in physical meaning. So the author tried to estimate the spot size based on the intensity distribution by using the pupil function of the electron wave optics approach. Scherzer (1949) have already given the estimation of resolving power and the contrast in the image of the conventional electron microscope by using the pupil function, though the chromatic aberration was not considered. Zeitler (1970) showed the image formation by using the aperture function (we generally call it the pupil function), however, the chromatic aberration was also not considered. Uchikawa and Maruse (1969 and 1970) tried to estimate the resolving power of the cathode lens based on the intensity distribution produced by the chromatic aberration. In this paper, the author tried to determine the spot size on the specimen by using the pupil function taking into consideration the chromatic aberration. The effect due to spherical aberration and defocusing was also considered. The model used in the present calculation was that concerned with the accelerating lens system composed of three anodes, and its spot size were estimated by the electron wave optics approach. Some discussion how to determine the spot size have also been dealt with.

§ 5-2-2 Theory of electron wave optics

The complex amplitude $h_a(r)$ on the image plane of the point object located on the optical axis in the object plane in Fig. 5-6 is given (in the case of rotationary symmetry system) by Huygens-Kirchhoff diffraction integral,

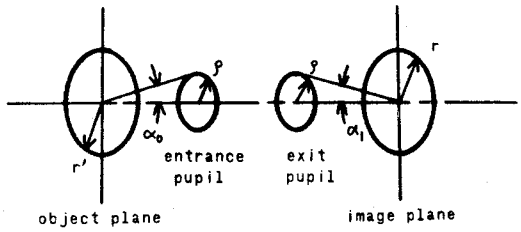

Fig. 5-6 Coordinate system of the electron wave optics.

$$h_a(r) = c\int_0^1 f(\rho)\ \rho\ J_0(r\rho)\ d\rho \quad , \tag{5-23}$$

where

c : constant,

$$f(\rho) = \tau(\rho)\exp[ik\omega(\rho)] \tag{5-24}$$

: pupil function (which is called "aperture function" by Zeitler),

$\tau(\rho)$: amplitude distribution in the exit pupil plane,

$k = 2\pi/\lambda$, λ : electron wave length,

$\omega(\rho)$: wave aberration of the electron optical system and ρ is the normalized radius in the exit pupil,

J_0 : zero order Bessel function of the first kind.

Then, the intensity distribution of the point object is given by

$$h(r) = h_a(r)h_a^*(r) = |h_a(r)|^2 \quad , \tag{5-25}$$

where $h_a^*(r)$ is the complex conjugate of $h_a(r)$.

The aberration included in these formulae is only of the wave type and the chromatic aberration is not dealt with. The author defined the intensity distribution I(r) on the specimen including the chromatic aberration effect as

$$I(r) = \int_{\lambda_{min}}^{\lambda_{max}} W(\lambda)\ \left|\ \int_0^1 f(\rho,\lambda)\ \rho\ J_0(r\rho)\ d\rho\ \right|^2 d\lambda \quad , \tag{5-26}$$

where $W(\lambda)$: weighting function.

In this section, it is assumed that the spherical, chromatic aberrations

and diffraction effect are dominant and the source size is regarded as point because the virtual source is negligiblly small as shown in the previous section. Let the wave aberration $\omega(\rho,\lambda)$ be expanded as follows (see Fig. 4-6 and Table 2-3).

$$\omega(\rho,\lambda) = \omega_{20}\rho^2 + \omega_{40}\rho^4 \quad , \qquad (5\text{-}27)$$

where

$$\omega_{20} = (\Delta z + z_0)\, a_p^2 / 2S_1^2 \quad , \qquad (5\text{-}28)$$

$$\omega_{40} = -M^4 C_s\, a_p^4\, (V_2/V_1)^{3/2} / 4S_1^4 \quad , \qquad (5\text{-}29)$$

$$z_0 = M^4 C_s\, a_p^2\, (V_2/V_1)^{3/2} / 2S_1^2 \quad , \qquad (5\text{-}30)$$

z_0 : least confusion plane for $\Delta V = 0$ eV as shown in Fig. 5-7,

$$\Delta z = C_c M^2 \Delta V / (V_1 V_2)^{1/2} \quad ,$$

and

$$\lambda = \{150 / (V_2 + \Delta V)\}^{1/2} \quad \text{Å} \quad ,$$

These values were calculated using geometric optics approach as was shown in Chap. 2, and the energy spread of the field emission was assumed as shown in Fig. 5-8.

In this method, a serious problem arises; it is very difficult to determine the spot size d of electron beam from the intensity distribution. The author defined the spot size d by the spread in which 80 per-cent of the total electron beam concentrates. In this case the central intensity of the electron beam is more than 80 per-cent of the central intensity with no aberration for the optimum aperture size which minimizes the spot size.

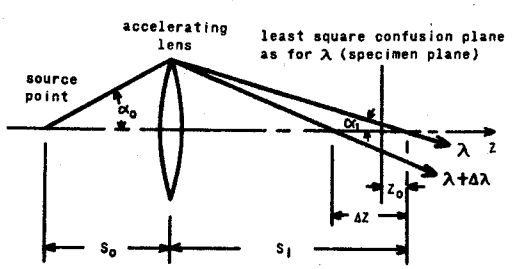

Fig. 5-7 Schematic diagram showing the aberration effect and its notations.

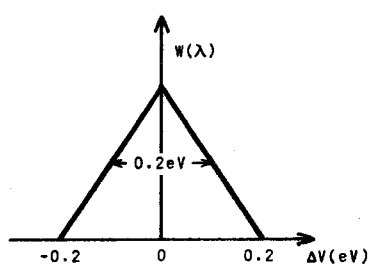

Fig. 5-8 Model of the energy spread of the field emission.

§ 5-2-3 Data and discussions for the three anode accelerating lens

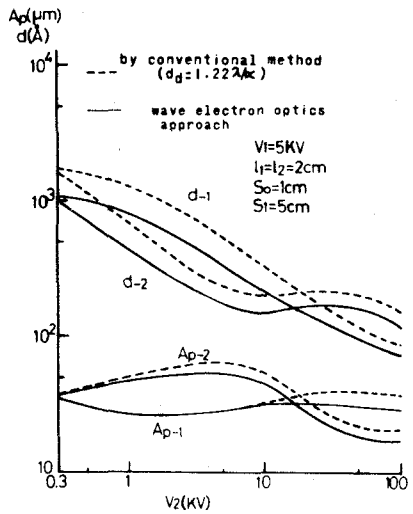

Fig. 5-9 Characteristics of the three anode accelerating lens.

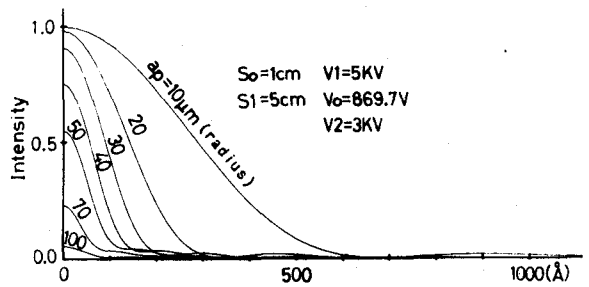

Fig. 5-10 Intensity distributions on the specimen for several aperture sizes.

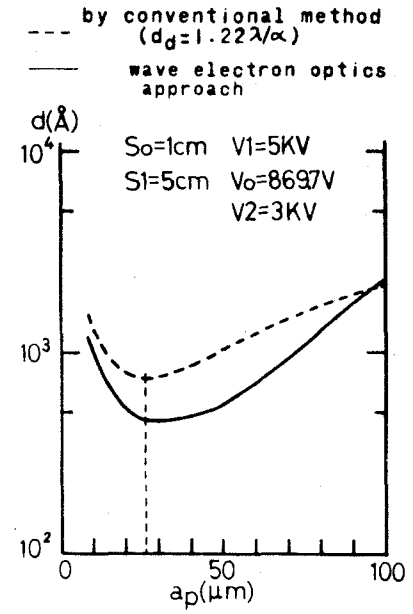

Fig. 5-11 Comparison of the spot size as the function of the aperture size.

The used model of the FE gun system and its notations are shown in Fig. 4-6. The optimum aperture radius which minimizes the spot size d defined in the preceeding section was automatically determined by using the Powell method (Powell 1964). The initial conditions presumed in these calculation were $L_1 = L_2 = 2$cm, $S_0 = 1$cm, $V_1 = 5$KV and $S_1 = 5$cm in Fig. 4-6. The energy spread is shown in Fig. 5-8, for the accelerating lens system composed of three anodes. Obtained results of the spot size d and the optimum aperture size a_p are shown in Fig. 5-9 and are compared with the results of the conventional method. In Fig. 5-10, the intensity distribution on the specimen is shown for several aperture sizes, and the comparison of the spot size between the conventional method and the wave electron optics estimation method is given in Fig. 5-11. From those results, following facts are noticed. (1) The values of the spot size for the conventional method are generally over-estimated and are less than twice as the value determined by the electron wave optics approach, if so much.
(2) The optimum aperture size was found almost of the same size by using the electron wave optics approach as shown in Fig. 5-9.
(3) The computation time of the spot size using the electron wave optics method is 10 ∿ 20 times of the conventional method.

§ 5-3 Effect of eccentricity of anodes

The influence of the eccentricity of electrostatic lenses on the spot size is analytically formulated and is numerically evaluated for the Butler type and the three anodes accelerating lens. For the aperture size which gives the minimum spot size, it is found that the misalignment less than 100μm between the anode axes in Butler type lens may be acceptable, but that in the case of three anodes type lens the misalignment should not exceed several tens μm.

§ 5-3-1 Introduction

Practically, in the assembling the accelerating lens system of the FESEM, it is impossible to set coaxially the optical axes of anodes without any eccentric misalignments and consequently the potential in the lens region is not axialy symmetrical. In this section the analytical formulation for evaluating the effect of the eccentricity of anodes (this effect is simply called the eccentric aberration in this thesis) and the allowable misalignments between the anode axes in the accelerating lenses of FESEM are presented.

The analytical formulae are derived neglecting the terms higher than the first in the expansion of aberration terms of the ray equation. The approximated value of a potential in the lens region is used because of difficulty of its exact estimation in asymmetric electrostatic field. The eccentric aberration of the Butler type and three anode accelerating lenses were estimated.

§ 5-3-2 Theory of the eccentric aberration

The paraxial ray equation is given by the following formula based on the principle of least action;

$$L[r] = r'' + \Phi' r'/2\Phi + \Phi'' r/4\Phi = 0 \quad , \qquad (5\text{-}31)$$

where r = r(z) is the radial coordinate and $\Phi = \Phi(z)$ is the axial potential. The ray equation including the aberration effect is expressed by the following formula

$$L[r] = P(r,\Phi) \quad , \tag{5-32}$$

where $P(r,\Phi)$ represents the aberration term. The general solution of Eq. (5-32) is given by

$$R(z) = R_0(z) + \varepsilon(z) \quad , \tag{5-33}$$

where $R_0(z)$ is the general solution of Eq. (5-31), and $\varepsilon(z)$ corresponds to the particular solution of Eq. (5-32). Then, the spread of the aberration W is generally expressed by (for example, Grivet 1965)

$$W = \varepsilon(z_i) = G\int_{z_0}^{z_i} (\Phi / \Phi_0)^{1/2} \; X \; P(X, Y, \Phi) \; dz \quad , \tag{5-34}$$

where z_0 and z_i represent the object plane and the image plane, respectively, Φ_0 is the potential on the object plane, G is the magnification of the lens, and

$$\begin{cases} X(z_0) = 0 \\ X'(z_0) = 1 \end{cases} \quad , \qquad \begin{cases} Y(z_0) = 1 \\ Y'(z_0) = 0 \end{cases} \quad . \tag{5-35}$$

From Eq. (5-34), we can obtain the spread of any aberrations due to the irregularity of the potential. However, it is not easy to determine $P(X, Y, \Phi)$, because it is generally very difficult to obtain exactly the irregular potential of the electrostatic lens. So $P(X, Y, \Phi)$ with respect to the eccentric aberration was determined as follows. Neglecting the terms higher than the first, the potential of the lens field was approximated by the following formula.

$$\begin{aligned} \phi(x,y,z) &= \Phi(z) - \{(x-\delta x)^2 + (y-\delta y)^2\}\Phi''(z) / 4 \\ &= \Phi(z) + xU_x + yU_y - (x^2 + y^2)\Phi''(z)/4 \end{aligned} \quad , \tag{5-36}$$

where

$$U_i = \Phi'' \, \delta i / 2 \quad , \quad (i = x, y) \quad , \tag{5-37}$$

and (x, y, z) is the rectangular-coordinate system. In the rectangular-coordinates, the ray equations are

$$\begin{cases} x'' = (1 + x'^2 + y'^2)(\phi_x - x'\phi_z)/2\phi & , \quad (5\text{-}38\text{-}a) \\ y'' = (1 + x'^2 + y'^2)(\phi_y - y'\phi_z)/2\phi & . \quad (5\text{-}38\text{-}b) \end{cases}$$

And, the trajectory without the aberration $R_i(z)$ $(i = x,y)$ is given by $R_i(z) = m_i X(z)$, where m_i's are the direction cosines of the initial velocity. So the ray equations including the aberrations are expressed from Eq. (5-32) by

$$\begin{aligned} L[\varepsilon_i] &= P_i(X, \Phi) \\ &= A_i^{(1)} + \alpha^2 A_i^{(2)} + m_i A_i^{(3)} + m_j A_i^{(4)} \\ &\quad + m_x m_y A_i^{(5)} + m_i^2 A_i^{(6)} \quad , \end{aligned} \qquad (5\text{-}39)$$

where

$$\begin{aligned} A_i^{(1)} &= U_i / 2\Phi \quad , \\ A_i^{(2)} &= (\Phi X'^2 + \Phi'' X^2/4) U_i / 2\Phi^2 \quad , \\ A_i^{(3)} &= -U_i^2 X / 2\Phi^2 \quad , \\ A_i^{(4)} &= -U_x U_y X / 2\Phi^2 \quad , \qquad (5\text{-}40) \\ A_i^{(5)} &= \{(U_j\Phi' - U_j'\Phi)X' + U_j\Phi'' X/2\} X/2\Phi^2 \quad , \\ A_i^{(6)} &= \{(U_i\Phi' - U_j'\Phi)X' + U_i\Phi'' X/2\} X/2\Phi^2 \quad , \\ (i, j) &= (x, y) \text{ and } (y, x) \quad , \end{aligned}$$

and α is the half- angle of the electron beam incident into the lens. Equation (5-40) was calculated neglecting the terms higher than the first in the expansion of the aberration terms. Then, from Eq. (5-34) the spread due to the eccentric aberrations E_i $(i = x, y)$ is given by

$$\begin{aligned} E_i &= H_i^{(1)} + \alpha^2 H_i^{(2)} + m_i H_i^{(3)} + m_j H_i^{(4)} \\ &\quad + m_x m_y H_i^{(5)} + m_i^2 H_i^{(6)} \quad , \end{aligned} \qquad (5\text{-}41)$$

where

$$H_i^{(k)} = G\int_{z_0}^{z_i} F_i^{(k)}(z)\, dz \quad , \tag{5-42}$$

and

$$F_i^{(k)} = A_i^{(k)} \chi (\Phi/\Phi_0)^{1/2} \quad , \tag{5-43}$$

$$\begin{pmatrix} i = x, y \\ k = 1, 2, ----, 6 \end{pmatrix} \quad ,$$

from Eq. (5-34).

From these equations it is shown that the incident electrons along the axis ($\alpha = 0$) are shifted by $\vec{D} = [H_x^{(1)}, H_y^{(1)}]$ in the Gaussian plane, and that the other electrons ($\alpha \neq 0$) are shifted by an additional amount

$$\vec{A} = (\alpha^2[H_x^{(2)} + H_x^{(6)}/2],\ \alpha^2[H_y^{(2)} + H_y^{(6)}/2]).$$

Hence the center of the spread due to the eccentric electrodes of the lens is shifted by $\vec{D} + \vec{A}$.

§ 5-3-3 Results and discussion

The effects of the eccentric aberration in Butler type and three anode accelerating lens are investigated by using the theoretical approach developed in the previous section. The models of the misalignments between the anode axes and the notations are shown in Figs. 5-12 and 5-13, respectively. Then we must determine the U_x and U_y for the calculations of the effects of eccentric misalignments in these two models. However, it is not easy to formulate them exactly. So the author approximated them as follows.

In the case of Butler type

$$\begin{cases} U_x(z) = 0 \\ U_y(z) = \Phi'' + (2z/L - 1)\delta/2 \end{cases} \quad , \tag{5-44}$$

and in the case of three anodes type

$$\left.\begin{aligned} U_x(z) &= \begin{cases} 0 & (0 \le z \le L_1) \\ \Phi'' + (z/L_1 - 1)\delta_{2x}/2 & (L_1 \le z \le L_2 = 2L_1) \end{cases} \\ U_y(z) &= \begin{cases} \Phi'' + (z/L_1 - 1)\delta_1/2 & (0 \le z \le L_1) \\ \Phi'' + (z/L_1 - 1)\delta_{2x}/2 & (L_1 \le z \le L_2 = 2L_1) \end{cases} \end{aligned}\right\} \quad (5\text{-}45)$$

The spreads due to the eccentric aberration by using these formula are shown in Figs. 5-14 and 5-15, respectively. The curves are for the misalignments of 10μm between the anode axes and the limiting aperture sizes located under the last anode which give the minimum spot size. In the figures "d" represents the spot size defined by Eq. (2-39) in Sec. 2-4. Only one eccentric type of error in the Butler type lens and three kinds of misalignments in the three anode accelerating lens are shown. From these curves, we found that the misalignment of 10μm does not produce the significant effect in both lenses. The effects of the misalignments between the anode axes in the lens models are shown in Figs. 5-16 and 5-17, respectively. From these figures, the misalignment less than 100μm between the anodes in Butler type lens may be acceptable, but in three anodes type lens the misalignments should not exceed several tens of μm. Especially in three anodes type lens it is noticeable that the misalignment between the first and second anodes is dominante. The spread due to eccentric aberration in this section is to be added to the spot size calculated by Eq. (2-39). When the aperture size is increased, the restriction on the misalignments, of course, becomes more severe.

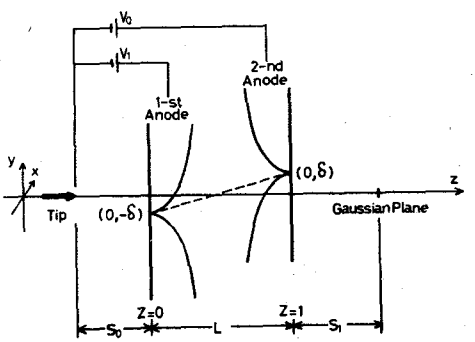

Fig. 5-12 Schematic diagram of the field emission gun with the Butler type accelerating lens.

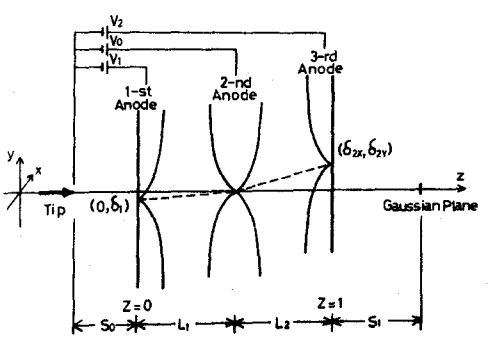

Fig. 5-13 Schematic diagram of the field emission gun with the three anode accelerating lens.

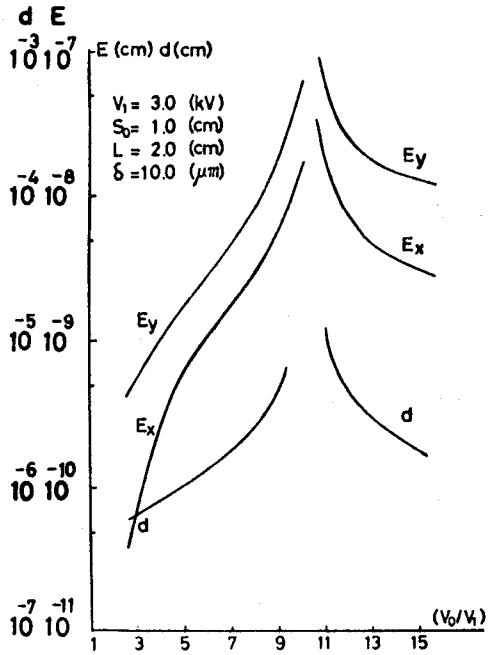

Fig. 5-14 The spreads of the eccentric aberration in the Butler type.

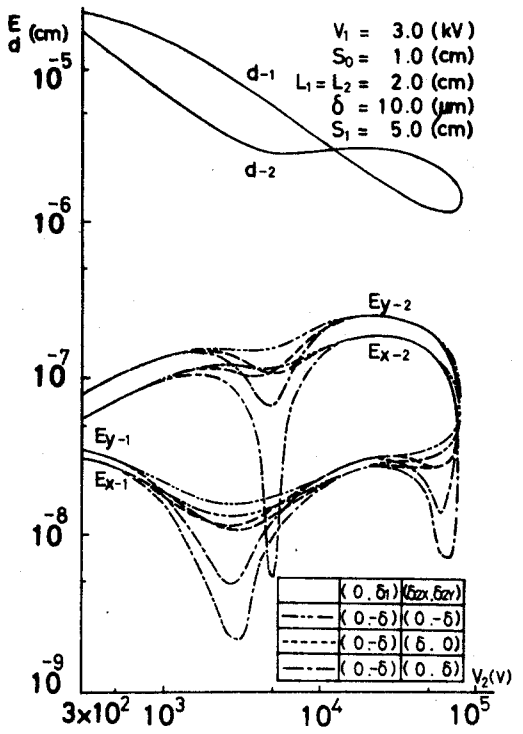

Fig. 5-15 The spreads due to the eccentric aberration in the three anode accelerating lens

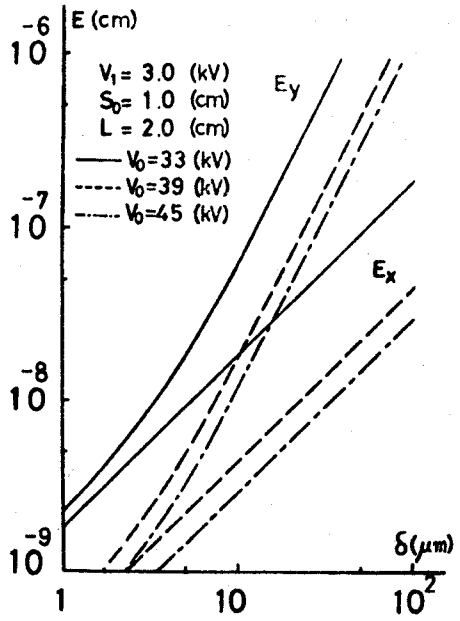

Fig. 5-16 The effects of the misalignments between the anode axes in Butler type accelerating lens.

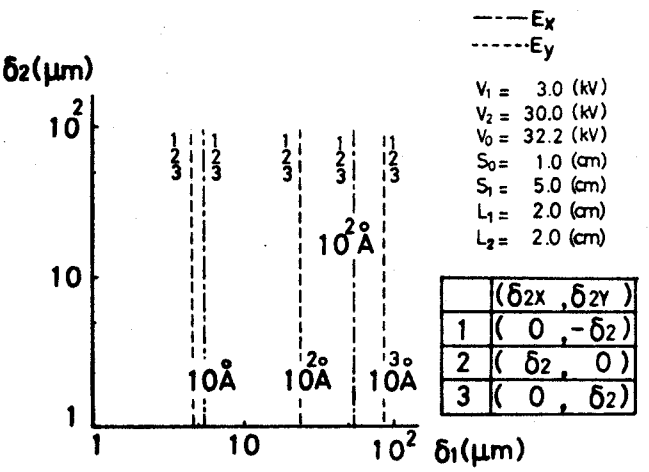

	(δ2x , δ2y)
1	(0 , -δ2)
2	(δ2 , 0)
3	(0 , δ2)

Fig. 5-17 The effects of the misalignments between the anode axes in the three anode accelerating lens. The spreads are shown by contour lines (this type of lens is characterized by two kinds of misalignments.).

CHAPTER 6 CONCLUSION AND SUMMARY

The contents are summerized chapter by chapter as follows:

Chapter 1

The accelerating lens for the FESEM is introduced and the purpose of the present investigation is described. The content of each chapter is also summarized.

Chapter 2

The theories and calculation methods which are necessary to the analyses of the characteristics of the accelerating lens and its electron optical system are described.

(1) It is necessary to know the electron trajectory in the analyses of the lens characteristics, and the potential and field in the lens region have to be obtained for the determination of the electron trajectory. So the principle of the mesh method, which is the most popular for the analyses of the potential and field among the given electrodes, is described, and it is described that this method can sufficiently be used for the analysis of the accelerating lens.

(2) The analysis method using electrode surface charges is suggested. This method has the advantage which can be dealt with open boundaries themselves. In the point of the accuracy this method is inferior to the mesh method, but it seems that this method can sufficiently be used in some fields.

(3) The theories and their calculation procedures of the electron trajectories, aberration coefficients of the lens, the spread of the electron beam (spot size) and the beam current on the specimen are described. (It is assumed that the spot size is mainly determined by the spherical, chromatic aberration, diffraction effect at the limiting aperture and virtual source size.) It is confirmed that these can be used with sufficient accuracy in the numerical computations.

Chapter 3

The characteristics of the Butler type and flat-plate accelerating lenses are analyzed and these are compared.

(1) The anode aperture effects which are very important in the analysis and design of the accelerating lens are analyzed. It

is shown that the anode aperture effects can be neglected in the Butler type lens, but in the flat-plate accelerating lens they cannot.

(2) According to the above mention, the characteristics of these accelerating lenses are analyzed and compared. In that conclusion it is found that the greatest advantage of the Butler type lens does not exist in small spot size (high resolution), but in the high current efficiency. Namely, as the small spot size is mainly determined by the characteristics of the auxiliary magnetic lens, the small spot size can well be obtained by using the flat-plate accelerating lens. These are also shown experimentally, and the computation results show satisfactory coincidence with experimental data.

Chapter 4

The new accelerating lens composed of three anodes is proposed.

(1) The conventional accelerating lenses are generally composed of two anodes. The working distances of these lenses are strongly dependent on the ratio of the emission and accelerating voltages. Namely, the working distance cannot be changed freely. However, the working distance can freely be changed by using the three anode accelerating lens. This means that the sufficient demagnification of the magnetic lens which is significant for generating the small spot size can be obtained even if the accelerating voltage is changed.

(2) The various conditions and their effects (the anode configurations, anode apertures, optimum aperture size, stability of the electric power source and so on) are discussed from the experimental standpoints.

(3) The computation data of this lens are compared with the experimental results. In these results a close coincidence is found.

(4) By the combination with the auxiliary magnetic lens this accelerating lens enourmously improves the current efficiency in the region greater than 10^{-9} amperes on the specimen, Especially, in the current region greater than 10^{-8} amperes the spot size is improved by at least one order of magnitude. This reason is

that the auxiliary magnetic lens can be operated under the optimum condition by the possibility of freely changing the working distance of the accelerating lens.

Chapter 5

(1) The virtual source size is evaluated for the conventional spherical model. However this model seems to be an oversimplified and unrealistic. So the sphere-on-orthogonal-cone model is examined as a realistic model of a point cathode electron source. In these results it is found that the conventional evaluation is slightly overestimated.

(2) It seems that the conventional definition of the spot size is rather poor in physical meaning. So the spot size is estimated from the intensity distribution by using the pupil function of the electron wave optics approach. In these results it is found that the conventional evaluation of the spot size is overestimated but the optimum aperture size is almost of the same order.

(3) One of the great causes which contribute to the reduction of the spot size is the effect due to the eccentric misalignment of the anodes. So the influence of the eccentricity of electrostatic lenses on the spot size is analytically formulated and is numerically calculated for the Butler type and three anode accelerating lenses. The results of this study show that the misalignment of 100μm for the Butler type may be acceptable, but in the three anode accelerating lens it seems that the misalignment should be less than tens of μm.

The resolution of the SEM is tremendously improved by using the FE gun. For high beam current regions (greater than about $10^{-9} \sim 10^{-8}$ amperes), however, this gun is at present inferior to the thermal electron gun in the point of the resolution. This would be the greatest defect of the FE gun. As an approach to overcome this problem the use of the three anode accelerating lens is suggested in the present thesis. In particular it is shown that the spot size of less than 100Å can be obtained for the beam current of 10^{-8} Amp.. This results is obtained under the condition of the emission current of 30μA/sr from the source. Recently the build-up and

remolding processing are developed, and the emission current of 300μA/sr is obtained (Someya et al. 1974). So the higher resolution will be acheived by using these techniques. This accelerating lens also has an advantage that the accelerating voltage can freely be changed without losing the characteristics of the magnetic lens. From these fact, it seems that not only in the field of conventional SEM but also in the field of investigations such as Scanning Auger Electron Microscope, Electrom Beam Microfabrication and so on the FE gun system consisted of three anode accelerating lens is expected to become a powerful tool in future.

ACKNOWLEDGEMENT

The author wishes to thank Prof. T. Suzuki for his interest in the present work, his kind advices and fruitful discussions during the course of this work.

The author would like to thank Prof. H. Hashimoto and Prof. S. Nakamura for their helps and fruitful advices to the present work.

The author wants to express his thank to Prof. R. Shimizu for his helps and suggestions during its completion.

Thanks are due to Dr. T. Komoda, Dr. M. Ichihashi, Dr. S. Nomura and Mr. Y. Nakaizumi of Hitachi Central Research Laboratory who gave invaluable advices for the construction of the apparatus.

The author acknowledges Prof. T. E. Everhart and Prof. J. C. Wiesner of California Univ. for their fruitful discussions and advices.

The author would like to thank Prof. H. Hamada of Okayama Univ. for his kind advices and discussions concerning the geometrical electron optics, and Prof. T. Kubo, Prof. S. Makinouchi, Dr. T. Torii and Mr. Y. Kasai for their kind helps and discussions with respect to the theories and numerical calculation methods.

REFERENCES

Angello J (1973) J. Franklin Inst. 296 403.

Ardenne M (1938) Z. Physik 109 553.

Brachet C (1946) Bull. Assoc. Tech. Maritime Aeron. 45 369.

Brewer G R (1971) IEEE Spectrum 8 23.

Broers A N (1970) In SEM/1970, IITRI, Chicago, Ill., p. 1.

---------- (1972) Proc. 5th Int. Conf. Electron Beam Technology, Houston p. 3.

---------- (1972) Rec. 10th Symp. on Electron, Ion and Laser Beam Technology, San Francisco Press.

Butler J W (1966) Proc. 6th Int. Cong. for E. M., Kyoto, p. 191.

Carre B A (1961) Comp. J. 4 73.

Castaing R and Guiner A (1949) Electron Microscope, Proc. Delft Conf., p. 60.

Cleaver J R A and Smith K C A (1973) In SEM/1973. IITRI, Chicago, Ill., p. 49.

Cosslett V E and Duncumb P (1956) Electron Microscope, Proc. Stockholm Conf.,

Crewe A V (1966) Science 154 729.

--------- (1967) Jour. Appl. Phys. 38 4257.

---------, Wall J and Welter L M (1968) Jour. Appl. Phys. 39 5861.

---------, Eggenberger D N, Wall J and Welter L M (1968) Rev. Sci. Inst. 39 576.

---------, Isaacson M and Johnson D (1969) Rev. Sci. Inst. 40 241.

--------- (1970) Science 12 1338.

--------- and Wall J (1970) Optik 30 461.

--------- (1970) Berichte der Bunsen-Gesellschaft 74 1181.

--------- and Wall J (1970) Jour. Mol. Bio. 48 375.

--------- (1970) Quar. Rev. Biophys. 3 137.

---------, Isaacson M and Johnson D (1970) Rev. Sci. Inst. 41 20.

---------- (1971) Rev. Sci. Inst. 42 411.

--------- (1973) Progress in Optics XI (V, Production of Electron Probes Using a Field Emission Source p. 223) North-Holland.

Cruise D R (1963) Jour. Appl. Phys. 34 3477.

Dyke W P et al. (1953) Jour. Appl. Phys. 24 570.

Elison M and Kudintseva G A (1962) Radiotekhn. Electron 7 1511.

EL-Kareh A B and EL-Kareh J C J (1970) "Electron Beam, Lenses, and Optics, vol. I", Academic Press.

Engel E, Kunath W and Krause S (1974) Proc. 8th Int. Cong. for E.M., Canberra, p. 118.

Everhart T E (1967) Jour. Appl. Phys. 38 4944.

---------- and Chung M S (1972) Jour. Appl. Phys. 43 3707.

Fraser D L, Meyers W J and Elser T G (1971) Rec. 11th Symp. on Electron, Ion and Laser Beam Tech., San Francisco, P. 209.

Glaser W (1940) Z. Phys. 116 56.

Gomer R (1961) "Field Emission and Field Ionization", Harvard Univ. Press.

Good R H and Muller E W (1956) "Handbuch der Physik, vol. 21", Springer-Verlag, Berlin.

Grivet P (1965) "Electron Optics", Pergamon Press.

Hamming R W (1962) "Numerical Methods for Scientist and Engineers", McGraw-Hill.

---------- (1969) J. Assoc. Comp. 6 37.

Hearle J W S, Sparrow J T and Cross P M (1972) "The Use of Scanning Electron Microscopy", Pergamon Press, Oxford.

Heddle D W O and Kurepa M V (1970) Jour. Phys. E. 3 552.

Higgins T J and Reitan D K (1951) AIEE Trans. 70 926.

Imhof R E and Read F H (1968) Jour. Phys. E. 1 859.

Kanaya K, Kawakatsu H and Ishikawa Y (1969) Bul. Electrotech. Lab. 33 1233.

Knoll M (1935) Z. Tech. Physik 16 467.

Koike H, Harada T, Goto T, Kokubo Y, Yamada K, Someya T and Watanabe M (1974) Proc. 8th Int. Cong. for E.M., Canberra, p. 42.

Komoda T and Saito S (1972) In SEM/1972, IITRI, Chicago, Ill., p. 129.

MacDonald N C, Robinson G Y and White R M (1969) Jour. Appl. Phys. 40 4516.

----------, Marcus H L and Palmberg P W (1970) In SEM/1970, IITRI, Chicago, Ill., P. 25.

---------- (1970) Appl. Phys. Letters 15 76.

---------- (1971) In SEM/1971, IITRI, Chicago, Ill., p. 91.

---------- and Waldrop J R (1971) Appl. Phys. Letters 19 315.

Marton M (1956) "Advances in Electronics and Electron Physics, vol. VIII", Academic Press.

McMullan D (1953) Proc. Inst. Elect. Engers. B100 245.
Munro E (1972) Proc. 5th Europ. Conf. on E. M., Manchester, p. 22.
Nomura S, Komoda T,Kamiryo T and Nakaizumi Y (1973) In SEM/1973, IITRI, Chicago, Ill., p. 65.
Oatley C W, Nixon W C and Pease R F W (1965) "Advances in Electronics and Electron Physics, vol. XXI", Academic Press.
---------- (1972) "The Scanning Electron Microscopy", Cambridge Univ. Press.
Pease R F W and Nixon W C (1965) J. Sci. Inst. 42 81.
Pierce J R (1949) "Theory and Design of Electron Beams", D Van Nostrand.
Plomp F H, Veneklasen L H and Siegel B M (1968) Proc. 4th Eur. Reg. Conf. on E. M., Rome, 1 141.
--------- (1972) Proc. 5th Eur. Reg. Conf. E. M., Manchester, p. 2.
Powell M J D (1964) Comp. J. 7 155.
Reimer L and Pfefferkorn G (1973) "Raster-Electron Microscopie", Springer-Verlag, Berlin.
Rose A (1948) Advan. Electron 1 131.
Ruska E (1933) Z. Physik 83 684.
Scherzer O (1936) Z. Physik 101 593.
---------- (1949) Jour. Appl. Phys. 20 20.
Septier A (1967) "Focusing of Charged Particles I" Academic Press.
Shaffner T J and Veld R D (1971) Jour. Phys. E 4 637.
Simon R (1969) In SEM/1969, IITRI,Chicago Ill., p. 445.
------- (1969) Jour. Appl. Phys. 40 2851.
------- (1970) ibid. 41 4632.
Singer B and Braun M (1970) IEEE Trans. Electron Devices ED-17 926.
Smith K C A and Oatley C W (1955) Brit. J. Appl. Phys. 6 391.
Someya T, Goto t, Harada Y and Watanabe M (1972) Proc. 5th Eur. Cong. on E. M., Manchester, p. 20.
----------, Yamada K, Koike H, Kokubo Y and Watanabe M (1974) Optik 40 (in press).
Swann D J and Kynaston D (1973) In SEM/1973, IITRI, Chicago, Ill., p. 57.
Swanson L W and Crouser L C (1969) Jour. Appl. Phys. 40 4741.
Tamura N and Shimizu R (1972) Tech. Rep. of Osaka Univ. 22 601.
Tonomura A (1973) Japan Jour. Appl. Phys. 12 1065.
Torii T and Makinouchi S (1968) Tech. Rep. of Osaka Univ. 18 287.
Uchikawa Y and Maruse S (1969) Japan Jour. Appl. Phys. 8 1359.
---------- (1970) J. Electron Microscopy 19 12.

Veld R D and Shaffner T J (1971) In SEM/1971, IITRI, Chicago, Ill., P. 17.
Veneklasen L H and Siegel B M (1970) Proc. 7th Cong. for E. M., Grenoble 2 87.
---------- (1972) Jour. Appl. Phys. 43 4989.
---------- (1972) Optik 36 410.
Weber B (1962/63) Philips Tech. Rev. 24 130.
Welter L M and Mcker A N (1972) In SEM/1972, IITRI, Chicago, Ill., p. 161.
Wiesner J C (1970) "Point Cathode Electron Sources, Part III", No ERL-70-6, Univ. of California, Oct..
---------- and Everhart T E (1973) Jour. Appl. Phys. 44 2140.
Widsor E E (1969) Proc. IEE 166 348.
Worster J (1970) Int. J. Electr. 28 117.
Young R D (1959) Phys. Rev. 113 110.
Zeitler E and Thomson M G R (1970) Optik 31 258.
Zworkin V K, Hiller J and Snyder R L (1942) ASTM Bull. 117 15.
---------- (1945) "Electron Optics and the Electron Microscope", John Wiley and Sons.

LIST OF PUBLICATIONS

1) K. Kuroda and T. Suzuki; "Aperture Effect of Electrostatic Lenses". Japan Jour. Appl. Phys., 11 (1972) 1222.

2) K. Kuroda and T. Suzuki; "Potential and Field Analysis Method Used Electrode Surface Charges", Japan Jour. Appl. Phys., 11 (1972) 1382.

3) K. Kuroda and T. Suzuki; "Electron Trajectory and Virtual Source of Field Emission Gun of SEM", Japan Jour. Appl. Phys., 11 (1972) 1390.

4) R. Shimizu, K. Kuroda, T. Suzuki, S. Nakamura, T. Suganuma and H. Hashimoto; "Field Emission Scanning Electron Microscope with Parallel Plate Gun Electrodes", IITRI, SEM/1973, Chicago, Ill., (1973) 73.

5) K. Kuroda and T. Suzuki; "Analysis of Accelerating Lens System in Field Emission Scanning Electron Microscope", Jour. Appl Phys., 45 (1974) 1436.

6) K. Kuroda, H. Ebisui and T. Suzuki; "Three Anode Accelerating Lens System for the Field Emission Scanning Electron Microscope", Jour. Appl. Phys., 45 (1974) 2336.

7) K. Kuroda and T. Suzuki; " Three Anode Accelerating Lens System for the Field Emission Scanning Electron Microsocpe (II)", Appl. Phys. Letters, 25 (1974) 23.

8) K. Kuroda and T. Suzuki; "Determination of the Spot Size by Using the Intensity Distribution in the Accelerating Lens System of Scanning Electron Microscope", Japan Jour. Appl. Phys., 13 (1974) 1636.

9) K. Kuroda, Y. Shingu and T. Suzuki; "Effect of Eccentricity of Anodes in Accelerating Lens for Field Emission Scanning Electron Microscope", Japan Jour. Appl. Phys., 13 (1974) 2033.

10) K. Kuroda and T. Suzuki; "High Current Efficiency Accelerating Lens System for Field Emission Scanning Electron Microscope", Jour. Appl. Phys., 46 (1975) (in press).

11) Patent: Inventor (T. Suzuki and K. Kuroda), Applicant (Hitachi Ltd.), Number of Application (487,914), Data of Application (January 19, 1973).